AFSWC-TDR-63-51

SWC
TDR
63-51

PARTICLE DISINTEGRATION STUDY FOR RE-ENTERING NUCLEAR AUXILIARY POWER SYSTEMS

Final Report
June 1963

TECHNICAL DOCUMENTARY REPORT NUMBER AFSWC-TDR-63-51

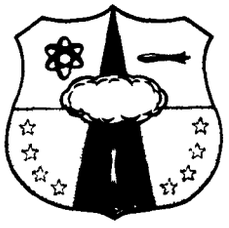

Development Directorate
AIR FORCE SPECIAL WEAPONS CENTER
Air Force Systems Command
Kirtland Air Force Base
New Mexico

Project No. 1831, Task No. 183101

(Prepared under Contract AF 29(601)-5004
by A. E. Levy-Pascal (Principal Investigator),
L. E. Bell, R. R. Koppang, A. H. Malinovsky,
S. W. Pohl, R. Silvestri, and N. A. Tiner,
Astropower, Inc., Newport Beach, Calif.)

HEADQUARTERS
AIR FORCE SPECIAL WEAPONS CENTER
Air Force Systems Command
Kirtland Air Force Base
New Mexico

AFSWC TDR-63-51

HEADQUARTERS
AIR FORCE SPECIAL WEAPONS CENTER
Air Force Systems Command
Kirtland Air Force Base
New Mexico

14 August 1963

ERRATA

AFSWC TDR-63-51. (U) PARTICLE DISINTEGRATION STUDY FOR RE-ENTERING NUCLEAR AUXILIARY POWER SYSTEMS

Page 24, Para 5.2.3: Change "(see Figure 24)" to read "(see Figure 29)."

Change "(see Figure 25)" to read "(see Figure 30)."

Page 69, line 12: Change K_d to K_D.

ABSTRACT

The purpose of this study was to determine the chemical history and related physical phenomena of liquid Zr-U droplets in the presence of a flowing mixture of atmospheric gases at various partial pressures.

A theoretical analysis of the aerodynamic and thermodynamic conditions affecting the droplets was carried out. Experimental investigation was conducted on the interaction of particles of 50- to 200-micron size with oxygen and nitrogen at different concentrations and total pressures.

The results obtained indicate that the droplets undergo partial or complete oxidation or nitridation, depending on experimental conditions. Only when oxygen was present did the droplets disintegrate into submicron particles. The frequency and mode of disintegration depend on the total pressure, oxygen concentration, and particle size; however, specific variables should be further investigated in order to reach more quantitative and realistic conclusions.

PUBLICATION REVIEW

This report has been reviewed and is approved.

John J. Ungvarsky

JOHN J. UNGVARSKY
Project Engineer

Philip C. McMullen

PHILIP C. McMULLEN
Major USAF
Acting Chief, Nuclear Power Branch

TABLE OF CONTENTS

LIST OF ILLUSTRATIONS

LIST OF TABLES

1.0 INTRODUCTION

Rapid progress in the development of nuclear auxiliary power (NAP) systems and their impending use in orbital flight applications have necessitated an investigation to demonstrate their safe and reliable disposal or recovery upon re-entry into the earth's atmosphere. The simplest, and perhaps the most practical means of NAP system disposal following mission completion would be to allow the unit to be destroyed by re-entry burnup. However, careful investigation, analysis, ground and flight testing, and possibly re-design must be accomplished to assure that the radioactive debris is safely dispersed at high altitudes. Accomplishment of this objective will allow the Air Force to effectively utilize nuclear auxiliary power units in the fulfillment of its space missions.

Some preliminary work has been done in the field of re-entry destruction of SNAP reactors (References 1 through 4). The most recent analysis of re-entry destruction of a reactor and the dispersion of its residue was conducted by AVCO under the technical direction of the Air Force Special Weapons Center, (Reference 5). This work included the investigation of the trajectory of the fuel elements, melting of the fuel elements, dispersal of molten residue, and combustion of the molten residue. Reference 5 points out a number of problem areas for further investigation. Most of these areas are at present in the last stages of investigation by various companies under contracts with the Air Force Special Weapons Center. Complementary investigations are being sponsored and directed by the Atomic Energy Commission.

The objective of the Astropower contract was to study the disintegration characteristics, chemical history, and related physical phenomena of molten zirconium-uranium alloy droplets that are ejected from the re-entering fuel rods. The molten droplet size range investigated was between 50 and 200 microns. The limits of investigation were defined by a number of mutually agreed-upon re-entry trajectories (prepared by General Dynamics/Astronautics) for fuel rods ejected from the NAP system at altitudes ranging from 250,000 to 50,000 ft (Reference 6). These fuel rod trajectories define only the starting point of the particle trajectories pertaining to this study.

Manuscript released by authors 10 April 1963 for publication as an AFSWC Technical Documentary Report.

A unique RF plasma apparatus was utilized for the experimental investigation of zirconium-uranium alloy particles. Particles of selected sizes were melted by passage through an argon plasma and were then subjected to reaction with oxygen or nitrogen diluted with argon.

This work included both theoretical analysis and an experimental investigation of the possible modes of droplet reaction and disintegration.

2.0 SUMMARY

This report presents results of a study of the chemical history and disintegration characteristics of molten zirconium-uranium droplets in the presence of flowing mixtures of oxygen and argon or nitrogen and argon at various partial pressures. The program was one of the phases of a larger study project pertaining to the safety aspects of nuclear auxiliary power systems re-entering the earth's atmosphere.

The experimental approach was to fluidize molten zirconium-10% uranium alloy particles (50 to 200 microns in size) in argon and react them with mixtures of predetermined concentration of oxygen or nitrogen in argon at total pressures varying from 0.092 to 1 atm. Data were obtained by high speed motion photography of the reacting particles, metallographic analyses of collected reaction products, and particle size comparisons before and after chemical interaction.

The mutually agreed-upon data (provided by General Dynamics/Astronautics) on fuel rod re-entry trajectories can only define the very initial conditions of a particle leaving the rod. A theoretical analysis was conducted to define the flow regime and conditions to which the expelled particles might be exposed at altitudes between 50,000 and 250,000 ft. The point of rod ejection and particle size will determine the regime, which might vary from molecular flow, through the transition region, to continuum flow. The ejected particles will exist under nonequilibrium conditions. The particle trajectories are unknown, and their definition is outside the scope of this study. However, the particles will undergo rapid deceleration, and most of them will probably remain in the rod wake. The pressure range to which these particles will be exposed was calculated to be between about 10^{-2} and 1 atm.

Results of this experimental investigation indicate that the molten droplets disintegrated only when oxygen was present and when the total pressure was about 1 atm or less. The disintegration processes are complex. When the pressure was about 1 atm, ablation, vapor-phase combustion, and condensation into submicron particles were observed. When the total pressure was between 0.4 and 0.95 atm, explosions were observed. The lower the total pressure, the greater the number of exploding particles. The explosion products were in the submicron range. However, the explosions

occurred after a definite initiation period starting from the time of oxygen introduction. The initiation period was less then 0.1 sec and decreased with decreasing total pressure and increasing oxygen concentration. Particles were observed to swell prior to explosion, a phenomenon which might be caused by the pressure differential between the inside and outside of the particle. In many cases hollow expanded spheres were collected as final products. Solid spheres were also collected from the same runs.

When only argon was present, the collected spherical products were shiny in appearance and of metallic composition with a very thin coating of oxide, which was caused by the impurities in the argon and some residual air in the apparatus. When oxygen was introduced, the zirconium was ultimately oxidized into zirconium dioxide, and the uranium into red-brown uranium oxide. The degree of completion of the oxidation reaction depended on experimental conditions. When nitrogen was introduced, the collected spherical products had gold-hued zirconium nitride cases, and the microstructure revealed a grain boundary network of precipitated nitrides.

The analysis of product particle size distribution showed a definite trend toward size reduction. However, these results are not quite satisfactory because the original particles varied considerably in shape, and their size distribution was too wide.

Specific recommendations have been made to solve these and other problems.

3.0 THEORETICAL ANALYSIS OF AERODYNAMIC FLOW REGIMES

At the start of this program, a series of fuel rod trajectories was prepared by General Dynamics/Astronautics (Reference 6). Although these trajectories define the conditions encountered by a re-entering fuel rod, they do not define the conditions of a molten droplet after it leaves the rod. The fuel rod surface and boundary conditions defined by the prepared trajectories are only the starting point of the liquid droplets' physical and chemical history. Considering the different courses that a droplet leaving the fuel rod might take, three probable alternatives can be distinguished: (1) the droplet might stay within the bow shock front of the rod, where exact conditions are unknown; (2) the droplet could cross the bow shock front and move into the free-flow stream; and (3) the droplet could be ejected or deflected into the wake zone of the rod where, again, the aerodynamic and thermodynamic parameters are unknown. Since more specific conditions cannot be determined at the present time, the range of variables to be considered is assumed to be between the free-stream and normal shock environments. In any event, after being ejected, droplets exist for some time under nonequilibrium conditions and decelerate more rapidly than the rods.

Since hypersonic flow conditions exist in the altitude range of maximum heat transfer and deceleration rate, the residence time of a particle as an entity within the strong shock field of the fuel rod is expected to be short. However, most of the particle reaction is expected to take place in the turbulent fuel rod wake.

The energy flux, momentum, and mass transfer to a particle are generally determined by calculating the dimensionless Knudsen and Reynolds numbers. The Knudsen number is the ratio of the body diameter to the average distance between molecular collisions. It is calculated from the kinetic theory relation (References 7 and 8)

$$K_n = \frac{\bar{l}}{D} = \frac{1}{\sqrt{2}\pi D\, n\sigma^2}$$

where

K_n = Knudsen number

D = Particle diameter, in.

$\bar{l}$ = Mean free path length, in.

n = Number density, molecules/in.^{3}

σ = Collision cross section, in.^{2}

Since it has not been established whether particle reaction will take place completely within or outside of the fuel element shock field, Knudsen numbers based on free-stream and normal shock conditions have been calculated (References 7 and 8) and are presented in Figures 1 and 2.

The results indicate that for varying particle sizes and altitudes, all types of aerodynamic flow regimes are possible. However, when the probable dispersal altitude range (Reference 5) is considered, it is seen from Figures 1 and 2 that the free molecule and transition regimes predominate for the particles of 50-micron to 200-micron size considered in this investigation. Furthermore, according to Reference 9, particles possessing radii below 30 to 60 microns would not cause radiation hazards.

The critical conditions required for simulation of free molecular flow have nevertheless been calcualted for marginal safety purposes and are presented in Figure 3. The critical conditions (the temperature, T, and pressure, P, at which free molecule flow is first encountered) are defined by (References 7 and 8)

$$K_n \text{ critical} \equiv 3\frac{\bar{l}}{D} = \frac{T}{4.24 \times 10^3 \, DP}$$

Parameters of particle diameter are shown for 50-, 100-, and 200-micron sizes. The area below any one of these curves is the free molecular flow regime, while the area above any curve is the transition region.

When the simplified trajectory and heating theory of Allen and Eggers (Reference 10) was applied, it was found that the predominant flow regime is described by hypersonic free molecular flow theory. In this regime, it is doubtful whether strong coupling can exist between the thermodynamic (combustion) and aerodynamic phenomena, irrespective of the particle size. Hence, the first criterion to be satisfied in the experimental simulation is that of the oxygen or nitrogen flux (or mass transfer) to the particle surface. The second criterion to be satisfied is that the energy balance approximates that of the simulated conditions. The mass flux to the particle will probably

control the rates of chemical reactions, and the energy balance will affect the particle temperature (and therefore the melting and vaporization processes).

Both mass and heat flux depend on the body shape, surface, and velocity ratio (a function of Mach number) in free molecular flow. The fundamental relationships are given in Reference 8. The mass flux equation is

$$\bar{N} = n_\infty \sqrt{\frac{RT_\infty}{2\pi m}} \iint_s \left\{ e^{-(\zeta \sin\theta)^2} + \sqrt{\pi}(\zeta \sin\theta)\left[1 + \operatorname{erf}(\zeta \sin\theta)\right] \right\} \frac{ds}{s} \qquad (1)$$

where

$\bar{N}$ = Average flux over surface, moles/sec-ft^2

n = Free-stream density, lb/ft^3

T = Free-stream temperature, $^\circ$R

m = Molecular weight, lb/mole

R = Universal gas constant

S = Body surface, ft^2

ζ = Velocity ratio

erf = Error function

θ = Angle between flight path and normal to surface

Equation 1 may be rearranged in order that the pre-evaluated integrals of Oppenheim (Reference 11) may be used

$$\bar{N} = n_\infty \sqrt{\frac{RT_\infty}{2\pi m}}\, 2\pi^{1/2}\, \zeta \int_s \frac{e^{-(\zeta \sin\theta)^2}}{2\pi^{1/2}\,\zeta} \frac{ds}{s} + \int_s \frac{\zeta \sin\theta\left[1 + \operatorname{erf}(\zeta \sin\theta)\right]}{2\zeta} \frac{ds}{s}$$

$$= n_\infty \sqrt{\frac{RT_\infty}{2\pi m}}\, 2\pi^{1/2}\, \zeta\, (\bar{G} + \bar{F})\ \frac{\text{moles}}{\text{sec-in.}^2} \qquad (2)$$

$\bar{G}$ and $\bar{F}$ are integrals defined in Reference 11. The first two terms in Equation 2 may be interpreted as the average gas kinetic flux to a particle at rest. The remaining terms correct for the effects of directed velocity. Rigorously speaking, the above equations apply to a single component rather than to a gaseous mixture; however, if the mean free path lengths and molecular weights of the

gas components are approximately equal, these equations will also hold for their mixtures. The choice of argon as carrier and plasma fluid satisfies the above requirements.

Assuming that there are no directed velocity effects in the apparatus (i.e., the difference in magnitude and direction between the velocity of the particle and that of the surrounding gas is zero), the average mass flux of O_2 to the surface is given by (Reference 8):

$$\bar{N}_{O_2} = X_{O_2}\, n_\infty \sqrt{\frac{RT_\infty}{2\pi m_{O_2}}} \quad \frac{\text{moles } O_2}{\text{sec-in.}^2} \tag{3}$$

Since we require that the mass flux of O_2 to the particle be identical to the simulated case

$$\frac{\bar{N}(\zeta)_1}{\bar{N}_2} = \frac{\left|X_{O_2}\right|_1 n_{\infty_1}\sqrt{RT_{\infty_1}}}{\left|X_{O_2}\right|_2 n_{\infty_2}\sqrt{RT_{\infty_2}}}\; 2\pi^{1/2}\; \zeta(\bar{G} + \bar{F}) \equiv 1 \tag{4}$$

where X_{O_2} is mole fraction of oxygen in the mixture, and the term

$$2\pi^{1/2}\, \zeta\, (\bar{G} + \bar{F})$$

is the correction for directed velocity. The function $\zeta\ (\bar{G} + \bar{F})$ has been calculated for the range of Mach numbers of interest and is shown in Figure 4. Thus, given the altitude and velocity conditions, the determination of the mass flux simulation is straightforward. The correction for high Mach numbers is seen to be quite substantial. For conditions within the shock field, where no directed velocity effects are possible (the particle velocity equals the gas velocity), Equation 4 becomes

$$\frac{\bar{N}_1}{\bar{N}_2} = \frac{\left|X_{O_2}\right|_1}{\left|X_{O_2}\right|_2}\; \frac{n_1\sqrt{RT_1}}{n_{\infty_2}\sqrt{RT_{\infty_2}}} \tag{5}$$

where the number density, n_1, and temperature, T_1, are evaluated at the local condition within the shock field.

In Equations 1 through 5, the assumption was made that all of the oxygen molecules colliding with a Zr particle react to form ZrO_2. This assumption may be modified so that the model is applicable over a larger

range of conditions by assuming that the reaction is characterized by some activation energy, E (i.e., a fraction, $e^{-E/RT}$, of the total number of oxygen collisions react to form ZrO_2). In addition, since free radicals have approximately zero activation energy, the frequency term can be modified to yield results under conditions where O_2 is dissociated. This approach is similar to that used by Hottel, et al. (Reference 12) in their study of carbon combustion.

Application of these assumptions to Equation 3 yields a reaction rate for Zr combustion of

$$\bar{N}_O + e^{-E/RT}\,\bar{N}_{O_2} = \left(X_O + X_{O_2}\,e^{-E/RT}\right)\frac{P}{(2\pi RmT)^{1/2}}\ \frac{\text{moles}}{\text{ft}^2\text{-sec}}$$

For the case of continuum flows, a simple combustion model can be formulated by considering the effects of a boundary layer on the combustion rate. The rate-limiting steps in this case are the diffusion of oxygen through the boundary layer, and a first-order reaction rate considering the oxygen partial pressure (as given in Equation 5) at the particle surface. The mass and chemical species balance equations may be written as follows (Reference 13)

$$\rho\,\frac{D\,Y'^{k}}{Dt} + \frac{\partial}{\partial x_j}\,\rho^k\,V_j^k = \dot{w}^k \tag{6}$$

$$\frac{\partial \rho}{\partial t} + \frac{\partial \rho\,\bar{V}_j}{\partial x_j} = 0 \tag{7}$$

where

ρ = Density, lb/ft^3

D = Particle diameter, ft

Y' = Species mass fraction

t = Time, sec

k = kth chemical species

V = Diffusion velocity, ft/sec

j = Flow coordinate tensor

$\dot{w}$ = Chemical reaction rate

$\bar{v}$ = Mass-weighted velocity of mixture, $\Sigma \frac{\rho^k}{\rho} V^k$, ft/sec

x = Position in particle boundary layer, ft

Assuming one-dimensional, steady diffusional currents through the particle boundary layer, no chemical reaction within the boundary layer ($\dot{w}^k = 0$), and a reaction rate at the particle surface given by Equation 5 yields

$$\rho \bar{V} \frac{dy'_{O_2}}{dx} + \frac{d}{dx}\left(\rho_{O_2} V_{O_2}\right) = 0 \tag{8}$$

$$\frac{d\rho\bar{V}}{dx} = 0 \text{ or } \rho\bar{V} = \text{constant} \tag{9}$$

$$y'_{O_2} + y'_{N_2} = 1 \tag{10}$$

Integrating Equation 8 between any arbitrary point in the boundary layer and the particle surface

$$\rho \bar{V}\left(y' - y'_{wO_2}\right) + \rho_{O_2} V_{O_2} - \rho_{O_2} V_{O_2}\Big|_w = 0$$

where w = conditions at the particle surface (wall). The boundary conditions are

$$\underline{\text{At the surface}},\ x = O,\ \rho\bar{V}\Big|_w = \rho_{O_2} V_{O_2}\Big|_w = y'_{O_2}\,\rho\bar{V}\Big|_w + \rho_{O_2} V_{O_2}\Big|_w \tag{12}$$

$$\underline{\text{At the outside of the boundary layer}},\ x = \zeta,\ y'_{O_2} = y'$$

Substituting Fick's Law ($\rho V = \rho\mathscr{D}\, dy'/dx$) and Equation 12 into Equation 11 yields

$$\rho\bar{V}(y' - y'_w) - \rho\mathscr{D}\frac{dy'}{dx} - \rho\bar{V}(1 - y'_w) = 0$$

or upon rearranging

$$\frac{dy'}{y - 1} = \frac{\rho\bar{V}}{\rho\mathscr{D}}\,dx \tag{13}$$

where $\mathscr{D}$ = G as diffusion coefficient

The term $\rho\bar{V}$ has been shown to be a constant (Equation 9). Assuming that the Schmidt number is one, $Sc = 1 = \mu/\rho\mathcal{D}$, then the product $\rho\mathcal{D}$ is equal to the viscosity, μ, which in turn is only a function of temperature, $\mu \propto T^{0.5 \to 0.66}$ Hence, for small temperature gradients across the boundary layer, the product $\rho\mathcal{D}$ is relatively insensitive to conditions within the boundary layer and will be assumed to have a constant value. Therefore, Equation 13 may be integrated between the edge of the boundary layer, δ, and the particle surface:

$$\ell n \frac{y'_\delta - 1}{y'_w - 1} = \frac{\rho\bar{V}}{\rho\mathcal{D}} \delta \tag{14}$$

The oxygen flux through the particle surface is equal to the rate at which the chemical reaction is proceeding:

$$\rho\bar{V}\Big|_w = \rho\bar{V} = -e^{-E/RT} \frac{Py'_w}{\left(2\pi \frac{R}{m} T\right)^{1/2}} \tag{15}$$

$$\ell n \frac{y'_\delta - 1}{y'_w - 1} = -\frac{e^{-E/RT} y'_w P\delta}{\left(2\pi \frac{R}{m} T\right)^{1/2} \mu} \tag{16}$$

Equation 16 may be used to evaluate the concentration of oxygen at the wall, y'_w. The conditions in the boundary layer (boundary layer thickness and pressure distribution) may be evaluated by assuming Stokes' flow around a sphere (Reference 14). These parameters are functions of particle diameter, Reynolds number, and free-stream velocity. Temperature, T, should be evaluated at the particle surface.

Equation 16 can be used for data correlation by setting $\delta = f(Re, \mu)$ and the activation energy, E, as unknowns which are to be determined from the experimental data. Note that the simulation requirements become more stringent for continuum flow as compared to free molecular flow due to the necessity to include Reynolds number as well as the ratio $P/T^{1/2}$.

Rigorous correlation of the theoretical and experimental data requires the knowledge of particle surface temperature as a function of time as well as the varying conditions of the immediate surrounding gas. Surface temperature

measurement is especially important, since its value will indicate the mode of reaction and is instrumental in the definition of the particle energy balance. Particle gas envelope composition, temperature, and pressure are required to estimate the mass and energy transport to the particle surface. These experimental measurements are extremely difficult to obtain on such small particles suspended in a moving gas stream under nonequilibrium conditions. On the other hand, experiments on such 40- to 200-micron reactive particles cannot be carried out satisfactorily by a static experiment, which allows them to rest on a solid support at such high temperatures, because they will interact with the support, and such experimental results will not realistically simulate re-entry conditions.

The exact and simultaneous experimental simulation of all parameters at any re-entry condition is impossible at the present state of knowledge; therefore, an approach must be adopted which is predicated upon practical experimental techniques. The approach selected was to describe the reaction characteristics of the molten fuel rod particles as a function of their initial size distribution as well as the experimental oxygen or nitrogen partial and total pressures. This information was utilized in the construction of a generalized reaction history which can be applied to any re-entry condition in the continuum flow regime.

4.0 EXPERIMENTAL WORK

4.1 Equipment

4.1.1 Plasma Apparatus

The plasma apparatus used is shown in Figure 5. A 7.5-kw Lepel high frequency generator produced a plasma by inductively coupling its energy to argon flowing inside a quartz tube. The plasma torch design was patterned after Reed's apparatus (Reference 15). During a typical experiment, prepared particles were dispensed by a special powder feeder, and the powder flow rate was controlled by an aspirator device. A water-cooled mixing chamber was located downstream of the plasma torch. A sharp-edged orifice, housed within the mixing chamber, allowed the plenum chamber pressure to be reduced while the plasma pressure was maintained at 1 atm. Secondary argon injection into the mixing chamber was utilized to control the plasma pressure. Reactive gases (oxygen or nitrogen) were injected tangentially downstream of the orifice. The plenum chamber (reaction chamber) was comprised of various lengths of Pyrex pipes and crosses. One of the crosses was fitted with an optically flat window for photographic purposes, and a second was provided with a door for product collection and removal. The chamber pressure was controlled by a series of bleed and restrictor valves located between the plenum chamber and the vacuum pump. An Ingersoll-Rand Model 7V vacuum pump was used for these experiments.

Gas flow rates were measured by Fisher-Porter volumetric flowmeters. The plasma pressure was monitored by a water manometer, and a mercury manometer was used for the measurement of the plenum chamber pressure.

Initially, molybdenum particles were passed through the plasma apparatus to prove the equipment's capability to melt Zr-10% U alloy particles when injected into the plenum chamber. Molybdenum was chosen because its melting point is higher than that of the Zr-10% U alloy. The molybdenum particles were found to be molten; they spattered upon impact on a glass microscope slide just downstream of the orifice.

The lack of basic design and performance information on RF plasma torches required the development of apparatus and procedures before reliable experimental work could be started. The initial plasma torch design utilized a technique of tangential argon injection to cool the quartz plasma tube and to maintain stable operation. Feasibility experiments conducted with molybdenum, and Runs 1-H and 2-H (Table II) were conducted with this design. It was found that this design was unsatisfactory because the particles passing through the torch had a tendency to be carried by the tangentially introduced argon stream into the relatively cool region existing between the plasma and the quartz tube wall. The final torch design, patterned after Reed's apparatus (Reference 15), eliminated this condition.

The structural integrity of the uncooled plasma tube was marginal. Any differential pressure across the tube wall caused the tube to distort or develop holes, which limited the plasma operating pressure to 1 atm. In order to obtain the reduced pressures required for experimentation, an orifice was placed downstream of the plasma tube.

The orifice design and diameter were found to affect the number and characteristic shape of particles collected. This caused difficulties in reaching accurate conclusions from the analysis of collected particles.

In order to eliminate the above difficulty, runs were conducted with and without the orifice to define its effect (see Table I). When a contoured nozzle was used, many of the molten particles contacted the wall and cooled prematurely. A sharp-edged orifice was found to eliminate the nozzle effect almost completely by allowing the particles that did not pass directly through the orifice to impact on its face and adhere to it. The orifice diameter was optimized to a point where enough particles for analysis could be collected satisfactorily within a reasonable length of run time.

The increase of orifice diameter resulted in a need for an increase in vacuum pumping capacity above that previously anticipated, and the vacuum pump available for the experimental program was not capable of producing the lower total pressures to simulate free molecular flow. The

total pressure range covered during this program was 1.35 to 14.7 psia (see Tables I and II).

4.1.2 Photographic Equipment

Two types of cameras were used to record particle behavior: (1) a model H-16 16 mm reflex Paillard-Bolex with variable shutter (maximum shutter speed of 1/640 sec, maximum film speed of 64 frames/sec, and Apochromat Kinoplik 25 mm lens), and (2) a W163269 16 mm Wollensak-Fastax (maximum film speed of 8,000 frames/sec, and a 50-mm Wollensak lens).

The Bolex camera was utilized for most of the film documentation, as it proved to be more economical and versatile. This camera is not fast enough to obtain sequence-type photographs except for cases of relatively low particle velocity; however, the single-frame photographs show a considerable number of disintegration characteristics which allow an interpretation of the reaction phenomena.

The Fastax camera was used during a few runs to obtain more detailed photographic data. Difficulties were encountered in camera setup, and some of the first film data were questionable.

The particle tracks obtained on the movie films were produced by radiation from the particles and did not show the actual particle. The track diameters were larger than the actual sizes of the particles. If the actual particles could be photographed with the same camera setup, the image produced would be about the size of a single film grain.

4.2 Procedures

4.2.1 Powder Preparation

Two different types of fuel rods were obtained from Atomics International Division of North American Aviation, Inc. for this experimental program: (1) zirconium hydride-10% natural uranium, and (2) zirconium-10% natural uranium alloy. These rods were reduced to powders and classified by the following procedure.

All the samples, files, holding jigs, sieves, and specimen containers were placed in a transparent plastic dry box. The dry box was purged with argon at a flow rate of 5 scfh for 16 hr. The fuel

rods were held over a container and filed by rubbing the rod over a Heller aluminum file. The collected powder was then classified by sieving through a 3-in. diameter U.S. Standard sieve series, consisting of the following meshes and corresponding screen openings:

Mesh No.	Screen Opening (Microns)
35	500
70	210
80	177
100	149
120	125
140	105
210	88
270	53
325	44

The desired isolated particle size cut was then inserted into the detachable plasma powder feeder inside the dry box, and the feeder was sealed, transferred, and connected to the plasma apparatus.

4.2.2 Operation of Plasma Apparatus

The operation of the plasma apparatus during a typical experimental run can be described by the following sequence of operations. The vacuum pump was turned on and the entire system purged with argon prior to opening the powder feed valve, so as to prevent contamination of the powder during startup. Following the 3- to 5-min purge, the powder feed valve was opened, and the primary argon flow control was set to the startup condition. The generator power was then turned on and the plasma initiated. All gas flows and pressures were set to give the desired run conditions, and the experimental variables were recorded. The powder feed was turned on for a typical run duration of approximately 5 min, during which movies were taken.

The apparatus shutdown procedure was to turn off the power, close the powder feed valve, turn off all gas flows, and stop the vacuum pump.

After an experimental run was completed, the collected products were removed from the apparatus and immediately subjected to microscopic examination. During the transfer and microscopic examination procedures, the particles remained immersed in an inert polytrifluorochloroethylene liquid in order to avoid any reactions with air.

4.2.3 Product Collection

During the majority of runs (refer to Table I), the products were collected in a metal dish filled with a chemically inert liquid. This liquid is a low molecular weight polytrifluorochloroethylene with a low viscosity (56 centistokes at 100°C) and low volatility. This technique proved very satisfactory for the collection of particles for microscopic and metallographic analyses.

Electron microscope samples were collected on thin 200-mesh screens coated with collodion substrate.

Early collection methods, utilizing glass microscope slides or wire screens coated with various substrates, were unsatisfactory for large particles, which would collide with the slide, disintegrate, and bounce off.

4.2.4 Metallographic Investigation

Preliminary analyses of collected particles were conducted by removing particles from the collection container, washing them with acetone, and mounting them on a glass microscope slide. These particles were inspected using various optical microscopes, and their photomacrographs were taken. The results of these analyses are presented in Section 5.0 of this report.

Preparation of sectioned particles for metallographic analysis was accomplished by the following procedure. Selected particles were first mounted in Bakelite. Rough wet grinding was carried out with abrasive papers of 240, 320, 400, and 600 grit. The final polish was done on an Eberbach five-speed polisher with micro cloth lap using 14-micron diamond paste, followed by 6-micron paste. Etching was accomplished by either of two methods: (1) use of a solution of 50 cc lactic acid, 10 cc HNO_3, and 3 to 5 drops of hydrofluoric acid (Reference 15), or (2) a solution of 47% concentrated nitric acid, 5% hydrofluoric acid (48% concentration), and 48% hydrogen peroxide (3% concentration) (Reference 17). Some slight variations in this procedure were necessary for the different types of products.

The X-ray diffraction analyses were done by the Materials Research and Process Engineering Section of Douglas Aircraft Co., Santa Monica Division.

4.2.5 Safety

An investigation of the health and fire hazards involved in the handling of Zr-U alloy powders was conducted. The aid of the Health Physics Dept. of Atomics International Division of North American Aviation, Inc., was obtained in the establishment of safety procedures and in the determination of the degree of hazard involved. A series of smear tests were taken, and samples were submitted to the Atomic International laboratories for analysis. Results of these tests showed an α count of 24 disintegrations per minute, and $\beta - \gamma$ counts ranging from 62 to 74 disintegrations per minute. These results revealed that the health hazard due to ingestion of Zr-U alloy powder was too low to warrant urine analysis or the wearing of film badges.

Astropower, Inc. Safety Standards and Procedures covering the handling of radioactive and pyrophoric materials were prepared. These standards follow similar procedures practiced by Atomics International Division of North American Aviation, Inc.

5.0 RESULTS AND DISCUSSION

5.1 Fuel Rod Material Analyses

The microstructure of the hydrided and unhydrided alloy samples is shown in Figures 6 and 7. The matrix of the hydrided sample consists of a banded or lamellar structure which is typical of zirconium hydride. Uranium is dispersed throughout the matrix and appears as a fine, black precipitate. It is probable that this precipitate is formed as hydrogen is added to the beta phase solid solution of uranium in zirconium, and that it contains a small amount of dissolved zirconium (References 17 and 18).

The microstructure of the unhydrided alloy consists principally of lamellar alpha zirconium solid solution and a few fine, black particles of alpha uranium precipitate. Some white spherical inclusions are noted which are probably zirconium carbide impurities. These impurities are not present in amounts that would affect experimental results.

The typical shapes and microstructures of the hydrided and unhydrided specimen powders before melting are illustrated in Figures 8b and 9b. The microstructures of the powders were found to be very similar to those of the rods from which they were prepared. Contamination of the powders due to handling was found to be negligible. The hydrided material was found to be very brittle, while the unhydrided material was somewhat ductile.

Photomacrographs of the prepared powders show the irregular shapes produced by the filing process (see Figures 8a and 9a). The classification of particle size by sieving allowed only for a two-dimensional discrimination; therefore, a long, thin particle passing through the sieve could have a much greater volume than a shorter and wider particle.

X-ray diffraction analyses of the original Zr-10%U alloy powder showed a hexagonal structure of alpha zirconium with approximate lattice parameters of $a = 3.232\text{Å}$ and $c_o = 5.147\text{Å}$ (see Table IV).

5.2 Analysis of Experimental Data

Experiments so far conducted utilized only oxygen or nitrogen as reactants mixed with argon at various partial and total pressures. These gases were used instead of air in order to try to elucidate the relatively simpler reactions prior to the more complex investigation with air, which

will be the next step (see Section 6.0). The investigation was conducted for three nominal particle sizes of 50, 100, and 200 microns. Data were obtained from the analyses of collected particles and from movie documentation of particle behavior. Data obtained from experiments conducted with the Zr hydride-U and Zr-U alloy particles showed identical results. This indicates that the Zr hydride-U particles lost all of their hydrogen while being heated within the plasma chamber, and that the material entering the plenum chamber was essentially Zr-U alloy. Since the results were identical and the Zr-U alloy is less pyrophoric, it was used for the majority of the tests.

Experimental conditions and movie photography observations are presented in Tables I and II. These tables give the variables under investigation; however, they offer only limited information for complete analysis of each of the disintegration processes observed. Experimental runs 72 and 73 produced the most useful information, which is presented and discussed in Section 5.2.2.

The fuel rod trajectory data presented by General Dynamics/ Astronautics (Reference 6) served as a basis for determining the total pressure range to be investigated. This range was calculated to be (for this particular study) between 0.092 and 1 atm of total pressure.

The only particle temperature control used during this study was the determination that the particle temperature was between the melting and boiling points prior to the introduction of oxygen or nitrogen.

5.2.1 Experiments Without Reactive Gases

Throughout the experimental program, spot check runs were made with argon and without reactive gases to obtain reference data and to determine possible air leakage into the system. Gas samples obtained from the plenum chamber during these experiments were subjected to spectroscopic analysis. The results of this analysis revealed oxygen and nitrogen partial pressures of 1.76×10^{-3} and 4.4×10^{-2} psia respectively. Such concentrations are considered to be negligible for this program.

These experiments produced mostly spherical particles with a very clean metallic appearance (Figure 10). The microstructure of these particles contained a much finer lamellar constituent than did the

original material (see Figure 11). The microstructure of collected particles from both hydrided and unhydrided powders was similar in appearance. This indicates the complete dehydrogenation of the hydrided zirconium. A very slight surface contamination which could be attributed to some gas impurity was noted in the microsections. X-ray diffraction analyses of these particles showed a hexagonal structure of alpha zirconium with approximate lattice parameters of $a=3.232\text{Å}$ and $c_o=5.147\text{Å}$ (Table V). These results are identical to those obtained for the original powders.

5.2.2. Reaction with Oxygen

Metallurgical macroexamination of particles collected from experiments during which oxygen was introduced showed the products to be consistently yellow glossy oxide spheres (Figure 14). The majority of these spheres were found to be completely oxidized and solid. A few particles were observed which did not completely oxidize. Figure 15 shows a particle on the left which is partially oxidized with metal still visible at the surface, and a split particle on the right with surface oxide and metal core. A solid oxide sphere is also shown in the center of the photograph for comparison. Such partially oxidized particles were most probably quenched in the collector before complete oxidation could take place.

A phenomenon was observed during which the particles expanded like a balloon and finally burst, as shown in Figure 16. This behavior was noted only at total pressures below 1 atm, and the number of expanded hollowed spheres collected appeared to increase with decreasing total pressure. Such hollowed spheres have been found as products of numerous other metallic powder combustion processes. Most available information has been summarized by Markstein (Reference 20).

Collected particles were sectioned and subjected to microscopic analysis. Particles which had been completely oxidized were porous, and a red or amber coloration was observed in the vicinity of the pores (see Figure 17). A number of these particles contained cavities, and a few were noted to have tunnels extending from the cavity to the sphere surface (see Figure 18). The expanded hollow spheres had very thin and brittle shells and could not be mounted intact or sectioned for further microscopic examination.

X-ray diffraction analysis of the completely oxidized particles showed a monoclinic lattice structure corresponding to the composition of zirconium dioxide (Table VI).

Very fine dust particles were collected on collodion-coated grids and subjected to analysis by electron microscopy. For the majority of runs, the grids were placed at the same distance from the plenum chamber inlet as the metal collection cups. These grids showed no collected particles. During run 2H (see Table II) the collecting grids were placed at a shorter distance, and a number of particles were collected (see Figure 19). These particles ranged in size from 0.02 to 0.10 microns. At 75 kv electrons can penetrate such thicknesses; therefore, the dark haloing effect shown in Figure 19 is not necessarily optical in nature but may be due to the presence of two different phases in the products, which possibly are metallic center and oxide cover. Unfortunately, fine particles were collected only on a few of the electron microscope grids, and only limited data were obtained.

Very fine dust particles collected during run 72 (see Table I) are shown in Figure 20. The particles agglomerated on the collecting grid indicate combustion in the vapor phase, but no electron diffraction patterns could be obtained to identify their composition.

Motion pictures of experiments conducted with oxygen revealed two phenomena. Some spallation and clouds of very small particles were observed to be expelled from the main particle track during total pressure conditions of about 1 atm (Figure 21). This behavior was considered to be ablative disintegration. However, when a cloud of smoke or very small particles is observed near a metallic particle undergoing combustion, this phenomenon is explained by a mechanism of metal evaporation followed by a gas-phase oxidation and condensation (see Reference 20). The second phenomenon was noted to occur at total pressures below 1 atm, where most of the particles were observed to explode (Figure 22). Figure 23 shows a sequence of two events during which the same particle appears to swell just prior to explosion (Figure 23a, upper particle) and subsequently explodes (Figure 23b). This observed swelling of a spherical particle might explain the history of the hollow expanded spheres collected. Such collected hollow spheres probably did not reach the stage of explosion. A characteristic of multiple explosions propagating from one particle was also noted and is shown in the left part of Figure 24.

Particle velocities were obtained from the known movie film speed and measured particle track length relationship (see Table I). During this part of the project a number of phenomena were photographed, but only limited data were available for complete analysis and interpretation of each case during Runs 1 through 71 (Table I).

A series of supplemental experiments designated as Runs 72 and 73 was conducted to better determine the initiation period prior to explosion as a function of oxygen partial pressure, total plenum chamber pressure, and particle size. Movie pictures revealed a wide distribution of particle velocities within constant limits during this series of experiments. The data handling and presentation were simplified by using the average velocity of the above limits (28 ft/sec).

Particle velocity measurements were made at a location below the orifice. Calculations were performed to determine whether the particles decelerated prior to the velocity measurement. This calculation involved an iterative solution to an approximation of the generalized Stokes' Law (see appendix for the actual solution). This equation does not allow for increase (or decrease) in particle mass or density resulting from chemical or physical processes, nor for the nonequilibrium temperature condition between the particle and the surrounding gas phase. The appendix shows, however, that the Stokes forces play a relatively minor role, and that a constant velocity approximation is justified for most of the experimental conditions.

The initiation period before explosion as a function of oxygen percentage by volume for particles about 50 microns in size at a constant total pressure is shown in Figure 25. These same data are presented as a function of total pressure at constant partial pressures in Figure 26. The data show that initiation time before explosion is strongly dependent on both total pressure and oxygen percentage.

These data were related to the composition of air (by volume). Data points were normalized by plotting the point on Figure 25, constructing a curve through the point and parallel to the experimental data, and obtaining a new value for residence time at the point of intersection of this curve and the 20.95% (by volume) oxygen line. These data and a faired curve are presented for 50-micron particles in Figure 27. Data for the 100- and 200-micron particle sizes were handled in the same manner. The faired curves for all three sizes are presented in Figure 28.

Initiation time before explosion is related to the overall role of the chemical process. Figures 25 to 28 indicate the following results: (1) an increase in oxygen concentration results in a decrease of initiation time, (2) an increase in total pressure results in a decrease of initiation time, and (3) larger particles require longer initiation times. It can be seen from these curves that the initiation time is very short, indicating that a particle leaving the fuel rod would explode in the rod's vicinity. Photographic results indicate that explosions did not occur at total pressures near 1 atm. Therefore, these curves do not apply to pressures close to 1 atm. This phenomenon is not yet fully understood. However, it seems that the pressure differential between the inside and outside of the particle is an important factor; the higher the pressure differential, the shorter the induction period and the higher the explosion frequency.

5.2.3 Reaction with Nitrogen

Collected particles from experiments utilizing nitrogen were found to be consistently golden in color. The surface of these particles was rough and exhibited a large depression similar to that noted in the shrinkage of metals during solidification under confinement (see Figure 24). The microsections of these particles revealed nitride casings and nitrides precipitated on the grain boundaries (Figure 25). X-ray diffraction analysis revealed a cubic zirconium nitride with lattice parameter a=4.65Å and primary alpha zirconium (Table VII). No fine dust particles were collected during these experiments.

Motion picture photography showed no indications of any disintegration phenomena during any of the nitrogen experiments. A comparison of the visible radiation intensities indicated that the particles' surface temperature was much lower during the nitrogen experiments than during the oxygen runs. It is evident that nitrogen reacts with the Zr-10%U alloy particles exothermally under the various experimental conditions summarized in Table I. However, it also appears that the heats of reaction are lower than those with oxygen, and that these reactions do not contribute directly to the disintegration of the investigated particles. Nevertheless, reactions with nitrogen should not be ignored, since they are certain to affect the results of the particles' interaction with air.

5.2.4 Product Size Distribution

A size distribution analysis was conducted for the various experimental conditions. This analysis was only partially successful because difficulties were encountered in collection and size measurement.

Particles detectable by optical microscopy were measured, and the data for various experimental conditions are presented in Table III. These data do not include the large hollow expanded particles, which were sometimes as much as 10 times the size of the mean. The particle size distribution was found to be fairly constant within the size ranges presented in Table III. It was noted that some of the collected particles were larger than the maximum sieve size of the original particles. This was attributed to the irregular shape of the prepared powders and the two-dimensional selection resulting from sieving.

The data suggest that some size reduction was encountered under all experimental conditions. However, these data are much too general to allow any quantitative conclusions to be drawn. One should start with a uniform shape and very narrow size distribution of the original particles in order to be able to obtain reliable data on the product size distribution. Furthermore, the increase in volume of the products due oxidation and nitridation should be considered, as well as the case of the hollowed expanded spheres. In the case of hydrided material there is some shrinkage due to hydrogen loss.

TABLE I

DATA SUMMARY FOR Zr-U ALLOY EXPERIMENTS

Run No.	Particle Size (Microns)	Chamber Pressure (Atm)	Pressure of Oxygen (Atm)	Pressure of Nitrogen (Atm)	Particle Velocity (Ft/Sec)	Residence Time (Sec)	Type of Nozzle	Photographic Observation*	Remarks
1	105-125	0.43	0.033	0	50-85	0.02-0.04	Contoured Nozzle	O and/or Δ	Product collection inadequate
2		0.33	0	0				□	
3		0.35	0.033	0				O Δ □	
4		0.32	0	0				□	
5		0.34	0.033	0	No data	No data		No data	
6		0.48	0.17	0					
7		0.37	0.066	0					
8		0.42	0.17	0					
9		0.36	0.066	0					
10		0.41	0.17	0					
11		0.83	0.296	0				Hit slide	
12		0.74	0	0	4-14	Not end of track		□	
13		0.86	0.308	0	No data	No data		No data	
14		0.78	0.278	0					
15		0.17	0	0					
16	53-105	0.132	0	0					Product collection by glycerine
17		0.092	0.0111	0	10-50+	Not end of track		Not end of track	
18		0.103	0.036	0	10-50+				
19		0.103	0.053	0	10-50+				
20		0.660	0.348	0	1-50+	0.5-2.5		O & □	
21		0.660	0.035-0.35	0	1-50+	0.5-2.5		O & □	
22	53-105	0.660	0.035-0.35	0	No data	No data		-	Product collection in halogenated liquid
23	105-500	1.0	0	0			None	-	
24		1.0	0.555	0				-	
25		1.0	0.385	0				-	
26		1.0	0.091	0	10-25	0.1-0.25		O?	
27	44-53	1.0	0.167	0	4-20	0.024-0.146		□ & Δ	
28	105-125	1.0	0.167	0		0.088-0.436		□ & Δ	
29		1.0	0.333	0		0.029-0.146		□ & Δ	
30		1.0	0.0815	0		0.088-0.436		□ & Δ	
31		1.0	0.333	0		0.025-0.125		□	
32		1.0	0.333	0		0.025-0.125		□ & Δ	
33		1.0	0.0815	0	No data	No data		-	
34		1.0	0	0.333	4-20	0.021-0.104		□	
35		1.0	0	0.0815		0.033-0.166		□	
36		1.0	0	0.308	No data	No data		No data	
37		1.0	0	0.333					
38		1.0	0.0815	0					
39	44-53	0.197	0	0			Contoured Nozzle		

*Key to photographic observation
O = Explosion
Δ = Ablation
□ = Dimming

TABLE I (CONTINUED)

DATA SUMMARY FOR Zr-U ALLOY EXPERIMENTS

Run No.	Particle Size (Microns)	Chamber Pressure (Atm)	Partial Pressure of Oxygen (Atm)	Partial Pressure of Nitrogen (Atm)	Particle Velocity (Ft/Sec)	Residence Time (Sec)	Type of Nozzle	Photographic Observation*	Remarks
40	44-53	0.197	0	0.033	No data	No data	Contoured Nozzle	No data	Product collection in halogenated liquid
41	105-125	0.197	0.033	0					
42		0.197	0.033	0					
43		1.0	0.167	0					
44		0.494	0.099	0			Sharp-edged orifice		
45		0.474	0	0					
46		0.474	0.0338	0	6-53+	0.03-0.25		O	
47	44-53	0.580	0.202	0	6-53+	0.01-0.81		O	
48		0.487	0.0325	0	13-53+	0.05-0.20		O	
49		0.487	0	0.0325		0.05-0.20		□	
50		0.552	0	0.193		0.05-0.20		□	
51	88-105	0.690	0.240	0	32-60+	0.03-0.05		O	
52		0.678	0.236	0	No data	No data		No data	
53		0.727	0.254	0				O	
54		0.710	0	0				□	
55	177-210	0.705	0	0				No data	
56		0.815	0.259	0	8-32	0.05-0.21		△ □	
57		0.776	0	0.238	No data	No data		No data	
58	88-105	0.776	0	0					
59		0.764	0	0.156					
60		0.724	0.217	0	20-25	0.10-0.125		O	
61	44-53	0.704	0	0	No data	No data		No data	
62		0.790	0.237	0	6-53+	0.008-0.06		O △	
63		0.783	0	0.235	No data	No data		□	
64	177-210	1.0	0	0			None	No data	
65		1.0	0	0.333	4-10	0.045-0.104		□	
66		1.0	0.333	0	4-13	0.045-0.145		△ □	
67		1.0	0.333	0	16-53	0.01-0.04	Sharp-edged orifice	△ □	
68	88-105	0.9	0.300	0	10-22	0.08-0.16		△ □	
69		1.0	0.333	0	4-13	0.03-0.08		△ □	
70		0.802	0.267	0	8-26	0.02-0.73		O	
71	177-210	0.869	0.124	0	14-30	0.09-0.20		O	
72	44-53	Var.	Var.	0	10-53	0.01-0.05		O	
73	44-53 88-105 177-210	Var	Var	0	No data	No data		O	

*Key to photographic observation
O = Explosion
△ Ablation
□ = Dimming

TABLE II

SUMMARY OF
Zr HYDRIDE-U PARTICLE EXPERIMENTS

Run No.	Particle Size (Microns)	Power Setting (%)	Total Chamber Pressure (Psia)	Partial Pressure of Oxygen (Psia)	Partial Pressure of Nitrogen (Psia)
1H	125-180	50	4.4	0	0
2H	125-180	50	4.4	0.016	0
3H	177-210	50	14.7	4.9	0
4H	177-210	50	14.7	0	0
5H	177-210	50	14.7	0	4.9

TABLE III

TYPICAL SIZE RANGE OF COLLECTED PARTICLES

Atmosphere	Argon			Argon-Oxygen Mixture**			Argon-Nitrogen Mixture		
Original Particle Size (Microns)	45-53	88-105	177-210	44-53	88-105	177-210	44-53	88-105	177-210
Final Spherical Combustion Product Size (Microns)	12-100			12-75*			25-75		
		25-105			12-75			50-150	
			25-200			50-200			50-200

* In some cases, no spheres were found. All particles disintegrated into fine dust after passing through the plasma flame.

** Large hollow expanded particles not included.

TABLE IV

X-RAY DIFFRACTION PATTERN OF
THE ORIGINAL Zr-10% U ALLOY POWDER

Relative Intensity (I)	Diffraction Angle (2θ)	d-Spacing o Measured (A)	ASTM Diffraction Data o (dA)	(hkl)
50	32.3	2.77	2.80	100
40	35.0	2.56	2.57	002
100	36.5	2.46	2.46	101
40	48.2	1.89	1.59	102
	51.2	1.78	1.62	110
40	57.0	1.61	1.46	103
50	63.7	1.46	1.40	200
40	69.0	1.36	1.37	112
	74.0	1.28	1.35	201
	82.3	1.17	1.29	004
	90.9	1.08	1.23	202
			1.17	104
			1.08	203

TABLE V

X-RAY DIFFRACTION PATTERN OF Zr-10% U ALLOY PARTICLES COLLECTED FROM ARGON EXPERIMENTS (RUN 64)

Relative Intensity (I)	Diffraction Angle (2θ)	d-Spacing Measured (Å)	ASTM Diffraction Data (dÅ)	(hkl)
	21.9	4.06	2.80	100
	28.5	3.13	2.57	002
	32.6	2.74	2.46	101
	35.3	2.54	1.59	102
100	37.1	2.42	1.62	110
	48.6	1.87	1.46	103
30	56.0	1.64	1.40	200
30	57.6	1.60	1.37	112
40	63.7	1.46	1.35	201
30	68.0	1.38	1.29	004
30	69.2	1.36	1.23	202
	70.2	1.34	1.17	104
	73.7	1.28	1.08	203
	78.3	1.22		
	82.4	1.17		
	9.15	1.08		

TABLE VI

X-RAY DIFFRACTION PATTERN OF Zr-10% U ALLOY PARTICLES COLLECTED DURING ARGON-OXYGEN EXPERIMENTS (RUN 28)

Relative Intensity (I)	Diffraction Angle (2θ)	d-Spacing Measured (Å)	ASTM Diffraction Data (dÅ)	(hkl)
	21.4	4.15	5.05	100
	24.0	3.70	3.69	011
100	28.1	3.17	3.63	110
80	31.5	2.84	3.16	111
20	34.1	2.63	2.84	111
20	34.9	2.57	2.62	002
	39.1	2.30	2.60	020
	40.7	2.21	2.54	200
	45.5	1.99	2.50	102
30	49.1	1.85	2.33	021
30	50.0	1.82	2.21	211
	54.3	1.72	2.19	102
	55.5	1.65	2.18	121
	58.3	1.58	2.02	112
	59.7	1.55	1.99	211
	61.1	1.52	1.55	022
	64.3	1.45	1.82	220
	66.6	1.40	1.80	112
	71.3	1.32	1.78	221
	75.3	1.26	1.69	300
				202

TABLE VII

X-RAY DIFFRACTION PATTERN OF Zr-10% U ALLOY POWDER PARTICLES COLLECTED DURING ARGON-NITROGEN EXPERIMENTS (RUN 65)

Relative Intensity (I)	Diffraction Angle (2θ)	d-Spacing Measured (Å)	ASTM Diffraction Data (dÅ)	(hkl)
30	31.7	2.82		
60	33.9	2.64		
100	36.4	2.47		
50	38.9	2.31	2.29	200
40	47.2	1.92		
	51.1	1.79		
80	56.5	1.63	1.62	220
60	62.7	1.48		
60	67.8	1.46	1.38	311
	70.6	1.33	1.32	222
	76.6	1.24		
	81.2	1.18		
	85.3	1.14	1.14	400
	89.3	1.10		
	94.5	1.05	1.05	331
	97.5	1.02	1.02	420

6.0 CONCLUSIONS AND RECOMMENDATIONS

Molten droplets which leave the surface of melting fuel elements of a nuclear auxiliary power system during re-entry will react with oxygen and nitrogen in the atmosphere, resulting in exothermic reactions. In this particular investigation the final chemical products were oxides and nitrides of zirconium, and a lesser amount of uranium. Like the chemical reactions, the other related phenomena are quite complex processes of ablation, vapor-phase combustion and condensation, hollow particle expansion, and explosion. A quantitative analysis of the degree of disintegration experienced by molten particles (50 to 200 micron) could not be obtained during this part of the program, although there is definite evidence of a trend toward size reduction. The explosion process which yields the highest degree of disintegration was partially defined as a function of the initiation time (initial rate of reaction), oxygen concentration, total pressure, and possibly the pressure differential between the inside and outside of the particle. Experimental results indicate that explosions occur only at total pressures below 1 atm and that the number of exploding particles increases as the total pressure decreases. It is believed, on the basis of the present results, that if a particle is completely molten upon leaving the fuel rod, it will undergo an explosion within less than 0.1 sec after its expulsion whenever its environment is between 0.4 and 0.95 atm total pressure (see Figure 28). When the total pressure is about 1 atm, ablation and vapor-phase combustion and condensation occur.

It is not yet possible to carry out a rigorous correlation of the theoretical and experimental data because critical parameters, such as particle surface temperature and uniformity of shape and size, were not obtained. Furthermore, the fuel rod trajectories (Reference 6) define only the starting points of the trajectories of the individual particles. Therefore, more complete knowledge of the variables affecting the particles, and a definition of their trajectories, would be of importance.

Due to the complexity of the problem and the large number of interacting variables involved, the investigation is still incomplete. It is recommended that this study be continued to further investigate the disintegration of fuel rod particles. Specific areas deserving special attention are: (1) particles of larger size, (2) lower total pressures, (3) measurement of particle surface

temperature, (4) interaction of particles with air, (5) the use of uniform shape and very narrow particle size distribution, and (6) improved correlation between theoretical analysis and experimental data.

REFERENCES

1. F. D. Anderson, "SNAP-2 Safety Evaluation," North American Aviation, Inc., report NAA-SR-417 (1 Jan 1960).

2. P. D. Cohn, "The Preliminary Investigation of SNAP-2 Re-entry Burnup," North American Aviation, Inc., report NAA-SR-4890 (12 Feb 1960).

3. P. D. Cohn, "The Preliminary Investigation of SNAP-10 Re-entry Burnup," North American Aviation, Inc., NAA-SR-MEMO-5036 (2 Mar 1960).

4. P. D. Cohn, "The Evaluation of the Simulated Re-entry Tests of SNAP-2 Fuel Elements conducted at Plasmadyne Corp.," North American Aviation, Inc., NAA-SR-MEMO-5159 (Apr 1960).

5. AVCO Corp., Research and Advanced Development Division, "Investigation of Re-entry Destruction of Nuclear Auxiliary Power Plants," Air Force Special Weapons Center Report AFSWC-TR-61-69 (Oct 1961).

6. General Dynamics/Astronautics, "Re-entry and Disposal Phenomena for Nuclear Auxiliary Power Systems," Third Quarterly Report, Contract AF29(601)-4893 (June 1962).

7. I. A. Schaaf and P. L. Chambre, "Flow of Rarefied Gases," Section II, Fundamentals of Gas Dynamics, ed by H. W. Emmons, Princeton University Press (1959).

8. W. O. Hayes and R. F. Probstein, Hypersonic Flow Theory, Academic Press (1959).

9. D. Sowle, "The Hazard Associated with the Dispersal of Small Particles from Re-entering Reactors as a Function of Particle Size," General Dynamics/Astronautics, Air Force Special Weapons Center Report AFWC-TDR-62-81 (Aug 1962).

10. H. J. Allen and A. J. Eggers, "A Study of the Motion and Aerodynamic Heating of a Missile Entering the Earth's Atmosphere at High Hypersonic Speeds," NACA TN 4047 (Oct 1957).

11. A. K. Oppenheim, "Generalized Theory of Convective Heat Transfer in a Free Molecule Flow, "J. Aero. Sci., 49-58 (Jan 1953).

12. C. M. Tu, H. Davis, and H. C. Hottel, "Combustion Rate of Carbon, Combustion of Spheres in a Flowing Gas Stream," Ind. and Eng. Chem., 26, 749-757 (July 1934).

13. S. S. Penner, Chemistry Problems in Jet Propulsion, Pergamon Press, New York (1957).

14. H. Schlichting, Boundary Layer Theory, Pergamon Press, New York, London, Paris (1955).

15. T. B. Reed, "Growth of Refractory Crystals Using the Induction Plasma Torch," J. App. Phys., 32, 12 (Dec 1961).

16. E. L. Foster, Jr., Letter describing procedures for preparing Zr-U Alloy samples for metallographic examination, Battelle Memorial Institute (Oct 1962).

17. F. E. Littman, "Zirconium-Uranium Combustion Study," Quarterly Report No. III, Air Force Special Weapons Center Contract No. AF29(601)-4954 (Oct 1962).

18. C. C. Wealsey, "A Nuclear Fuel Element for Space Application," Materials Science and Technology for Advanced Applications, Golden Gate Metals Conference, San Francisco, 1962.

19. J. B. Vetrano, "A Uranium Dispersion, Zirconium Hydride Matrix, Fuel for Compact Space Power Systems," Atomics International Div. of North American Aviation, Inc., presentation to the American Nuclear Society (Dec 1960).

20. G. H. Markstein, "Combustion of Metals," American Rocket Society Seventeenth Annual Meeting, paper No. 2657-62 (Nov 1962).

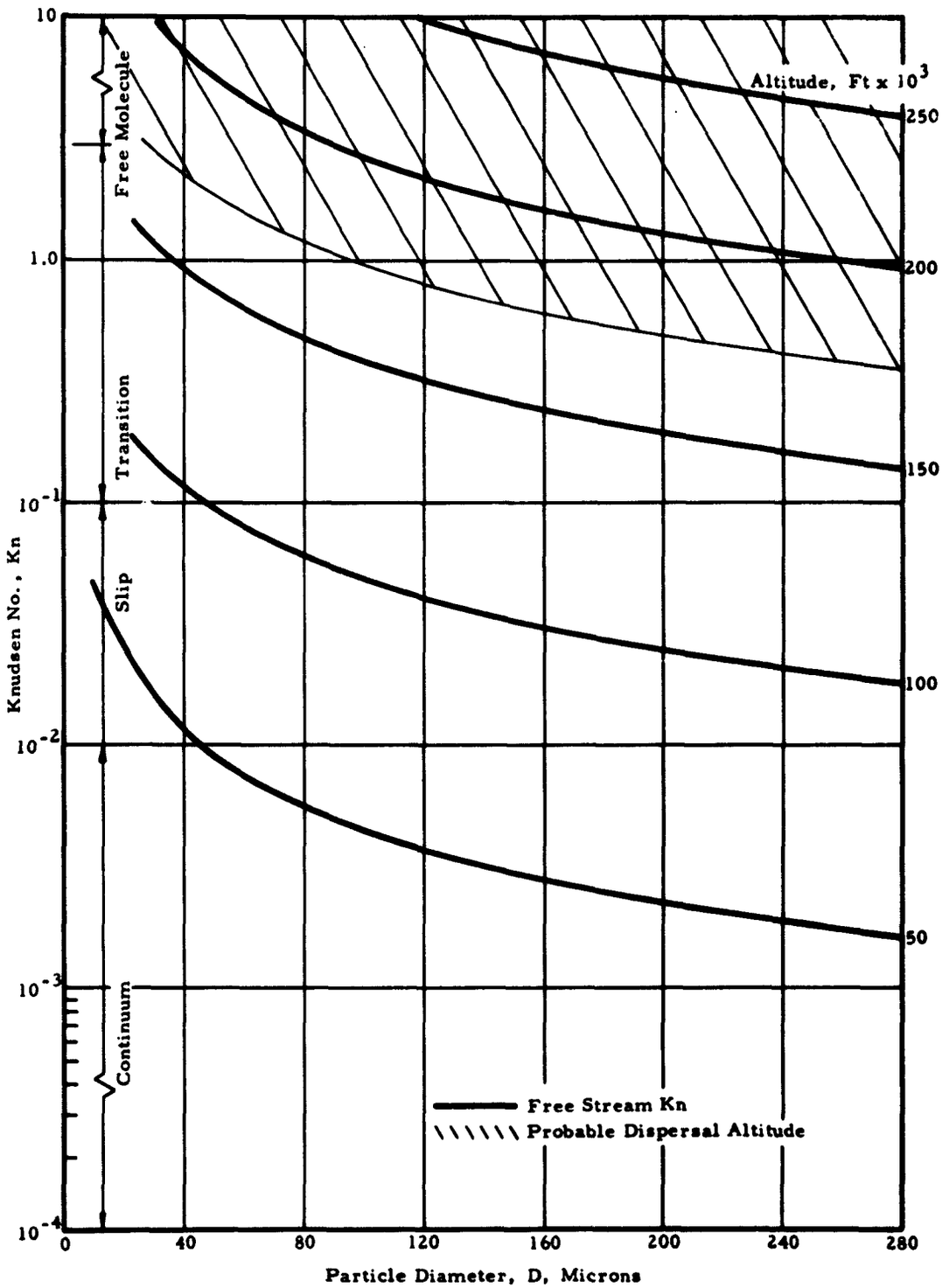

Figure 1. Flow Regimes of Particle Reaction Knudsen Numbers Based on Free Stream

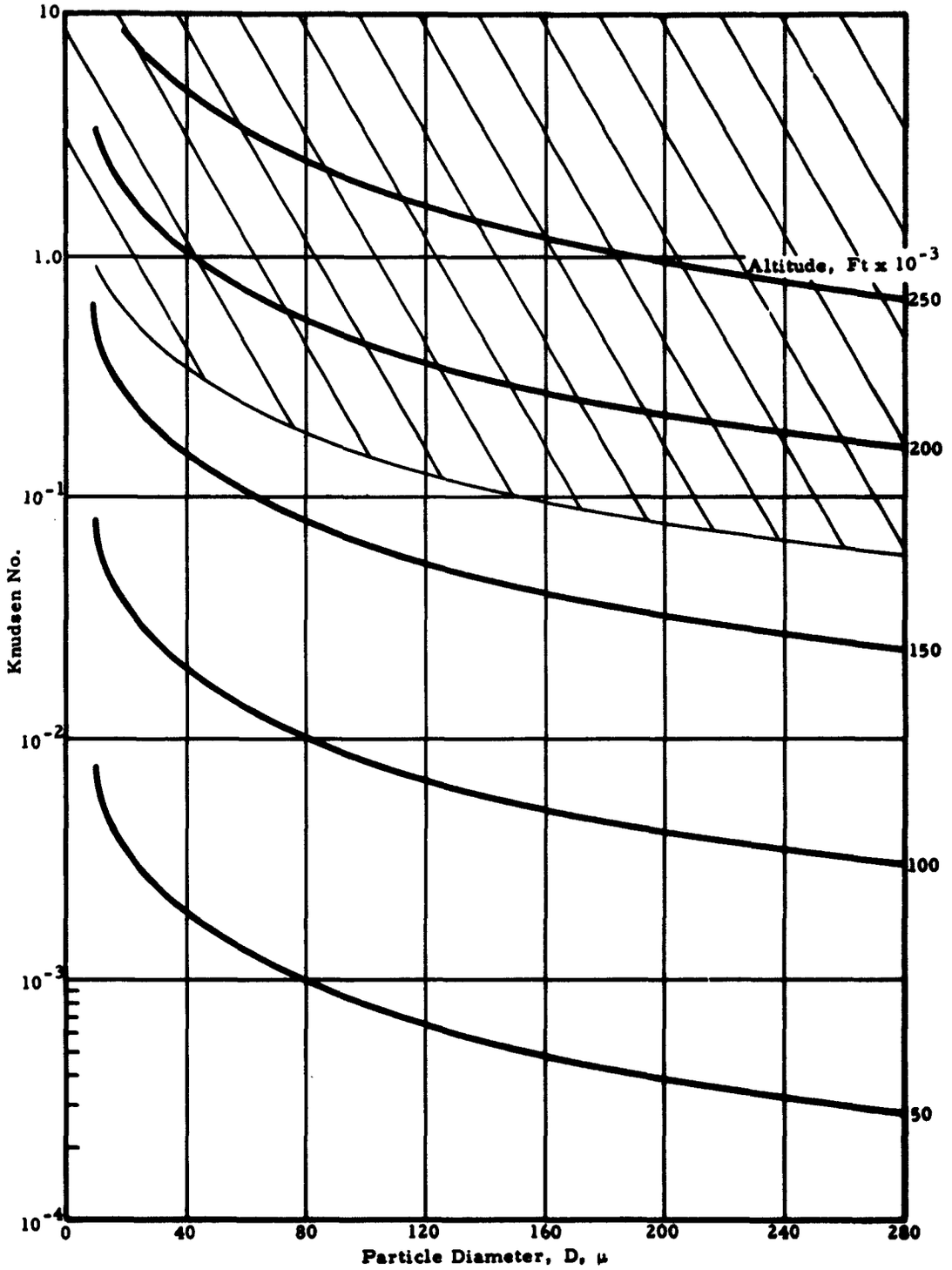

Figure 2. Flow Regimes for Particle Destruction Knudsen Number Based on Conditions Behind Normal Shock

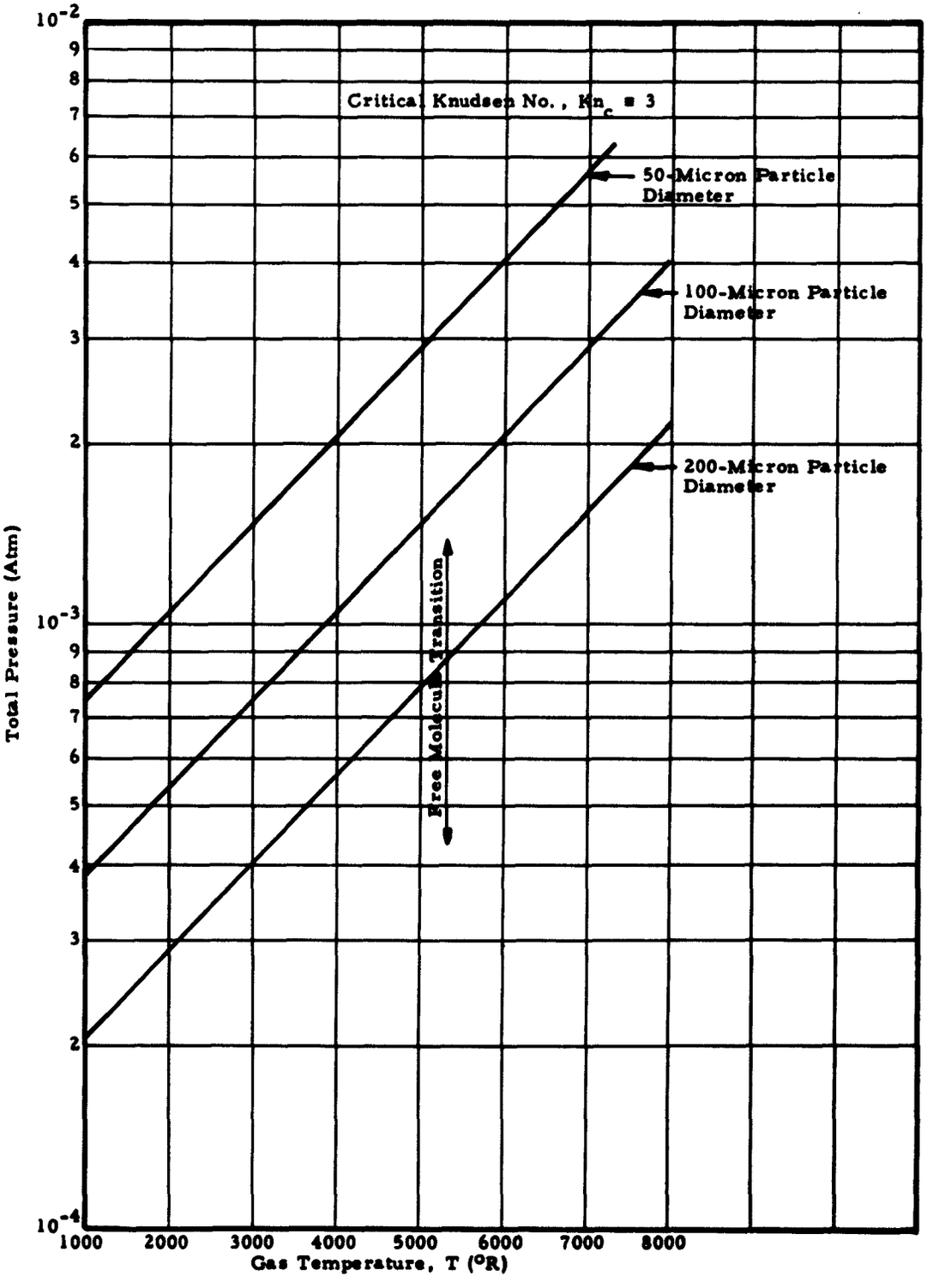

Figure 3. Critical Conditions for Free Molecule Flow

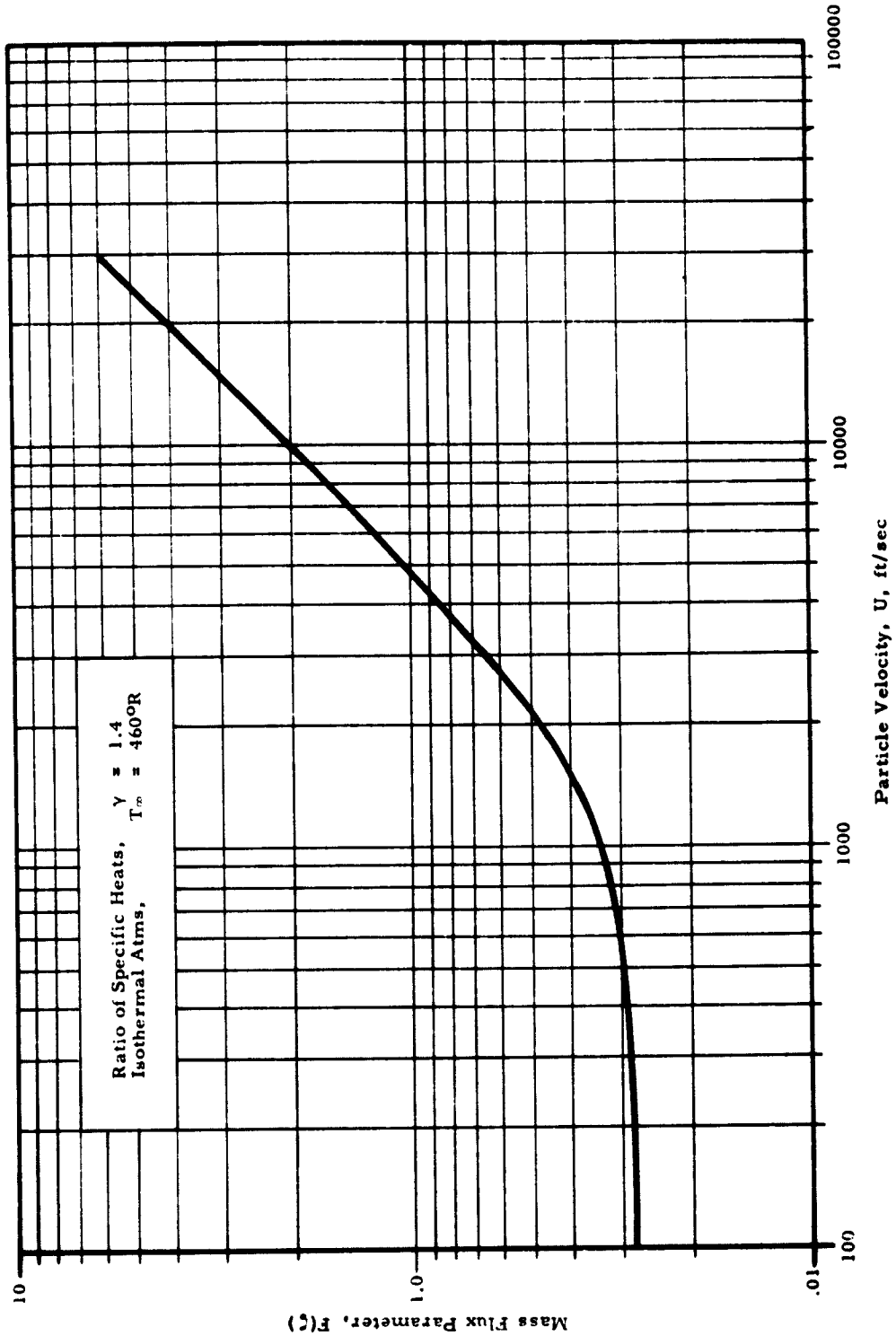

Figure 4. Mass Flux Correction Parameter, Sphere in Free Molecule Flow

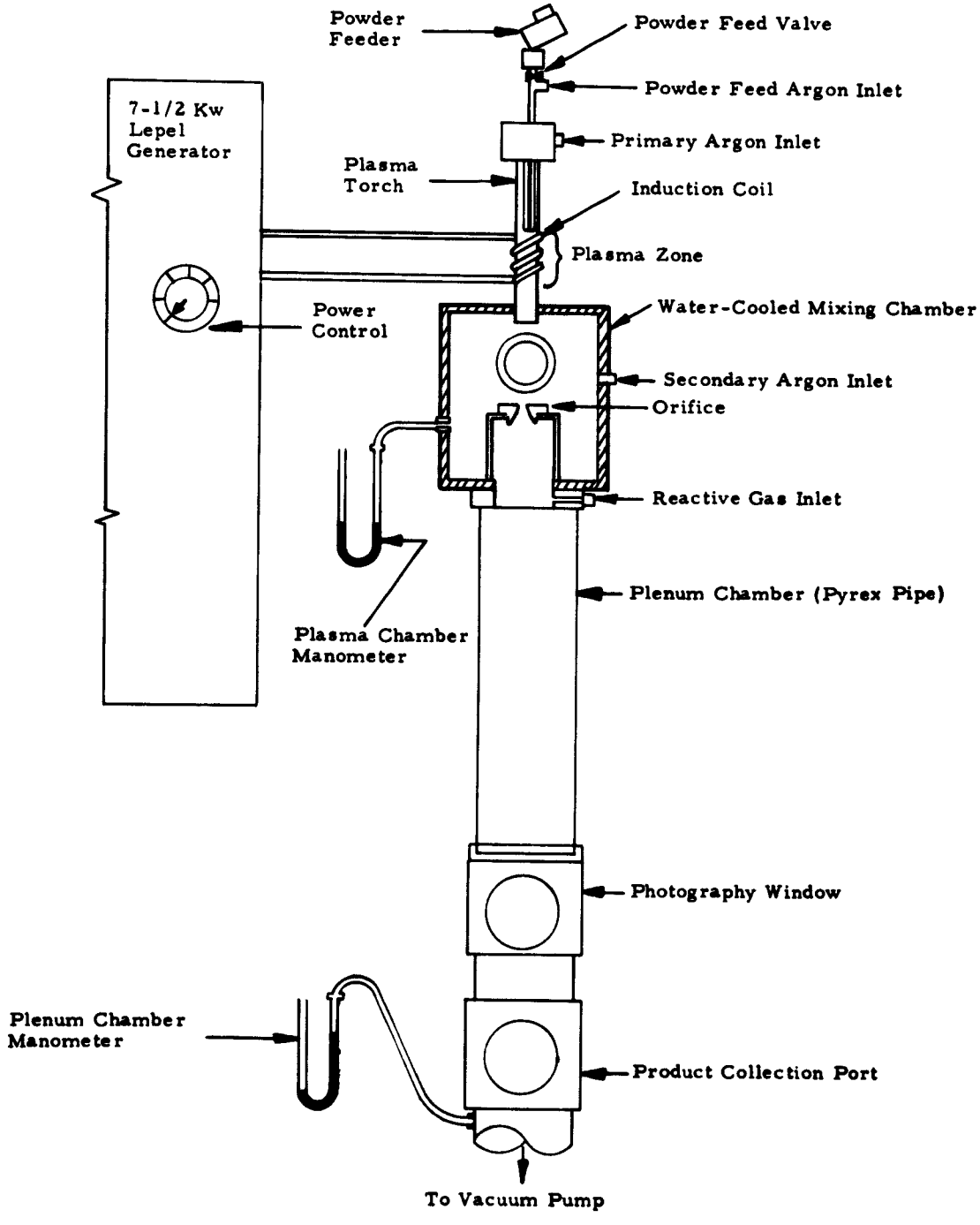

Figure 5. Plasma Apparatus

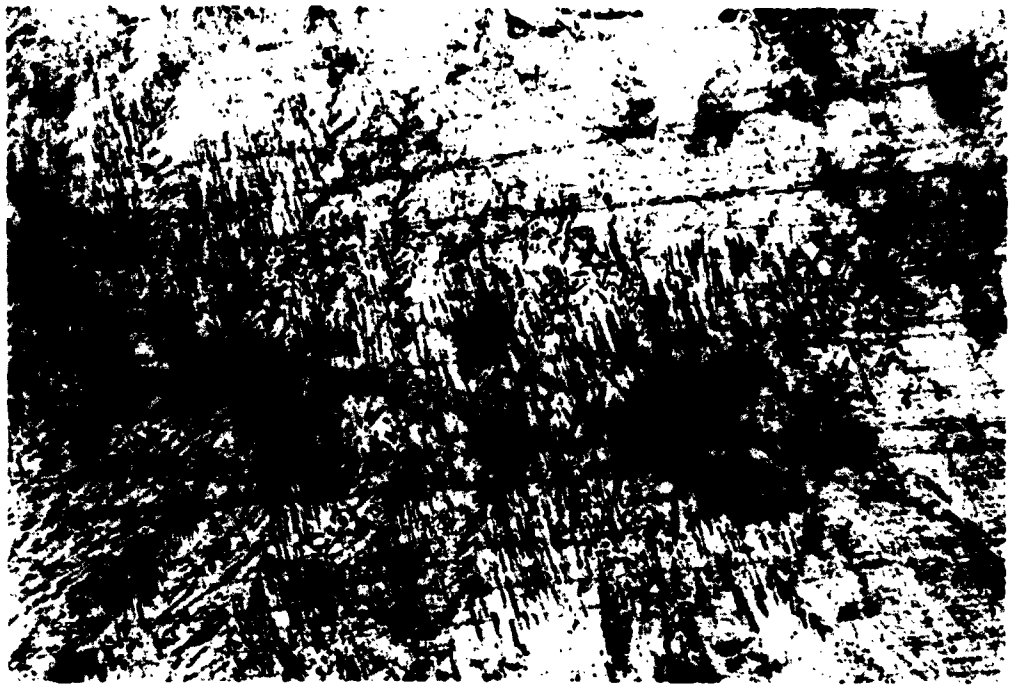

a. Magnification 200X

b. Magnification 700X

Figure 6. Photomicrographs of Zr Hydride-10% U Sample Showing the Lamellar Structure of Zr Hydride and Fine, Black, Dispersed Particles of Uranium. Etched with Aqueous Solution of HNO_3-H_2 F_2

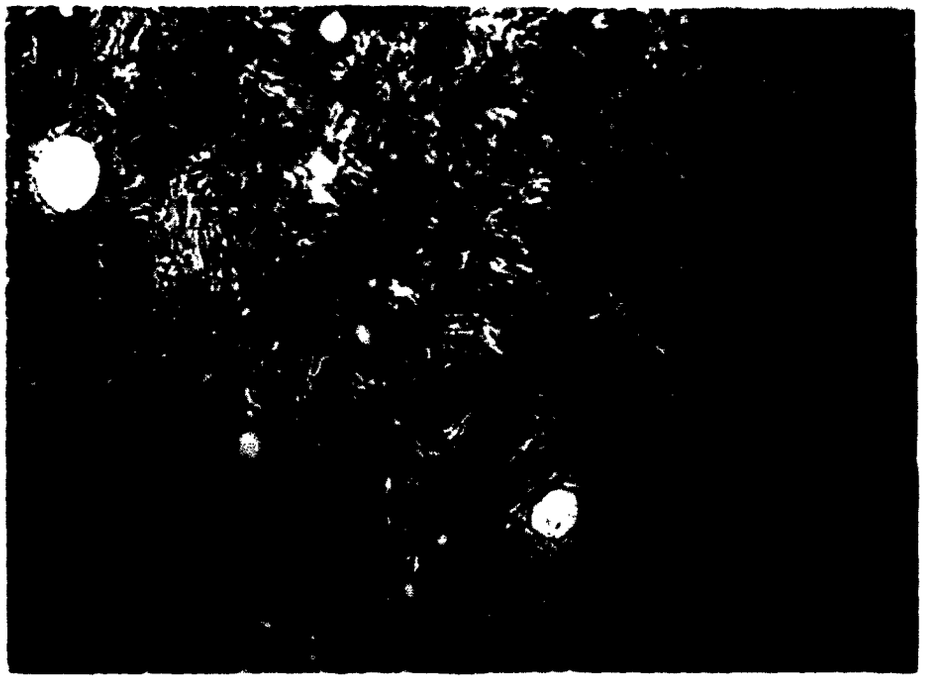

Figure 7. Photomicrograph of Zr-10% U Alloy Etched with Aqueous Solution of HNO_3-H_2 F_2

a. Magnification 50X

b. Magnification 700X

Figure 8. Photomicrographs Showing Shape and Microstructure of Zr Hydride-10% U Particles Collected at -35 +80 Mesh Sieve

a. Magnification 200X

b. Magnification 700X

Figure 9. Photomicrographs Showing Shape nd Microstructure of Zr-10% U Alloy Particles Collected at -12[illegible] +140 Mesh Sieve

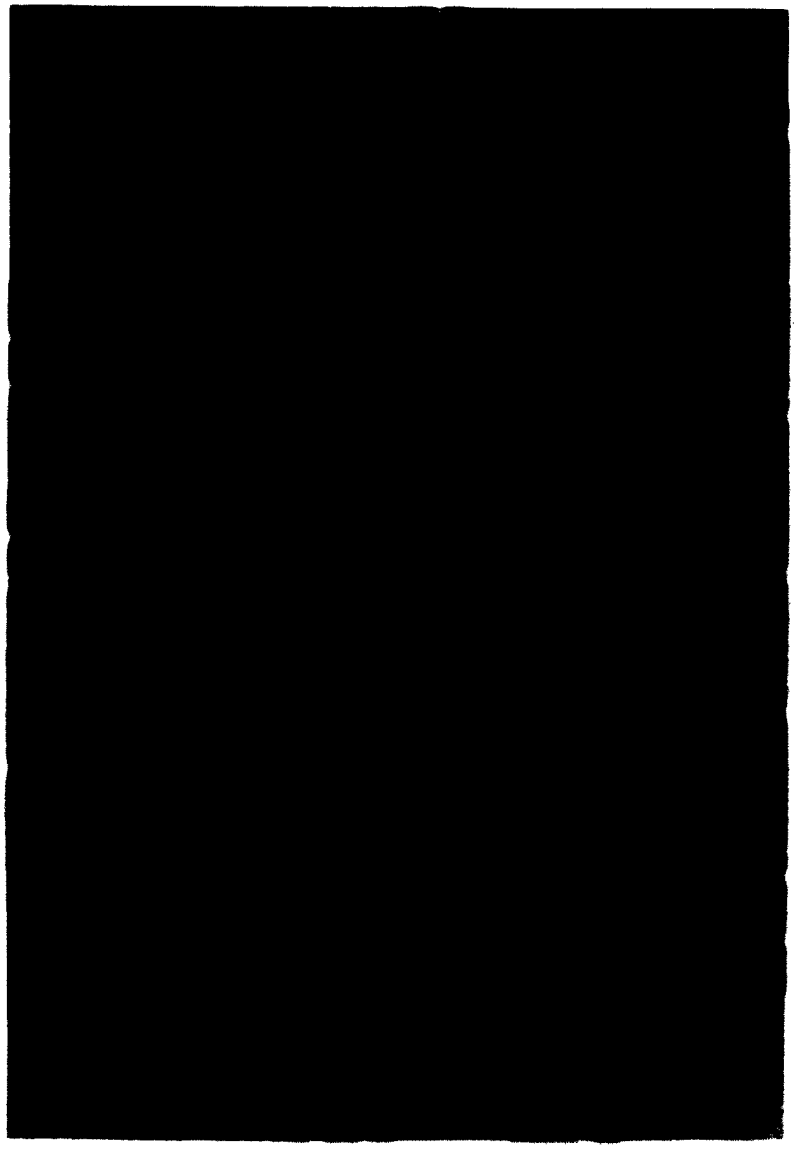

Figure 10. Photomacrograph of Typical Spherical Particles Collected from an Experiment During Which No Reactive Gas Was Introduced (Run 64)

Magnification 60X

Figure 11. **Photomicrograph Showing the Microstructure Typical of a Spherical Particle Collected from an Experiment During Which No Reactive Gas Was Introduced (Run 64)**

Magnification 700X

Figure 12. Photomicrograph Illustrating Surface Oxidation (Run 55)

Magnification 700X

Figure 13. Photomicrograph Illustrating Surface Oxidation with a Hollow Metallic Core. Note the Tunnel Through the Oxide Crust (Run 64)

Magnification 700X

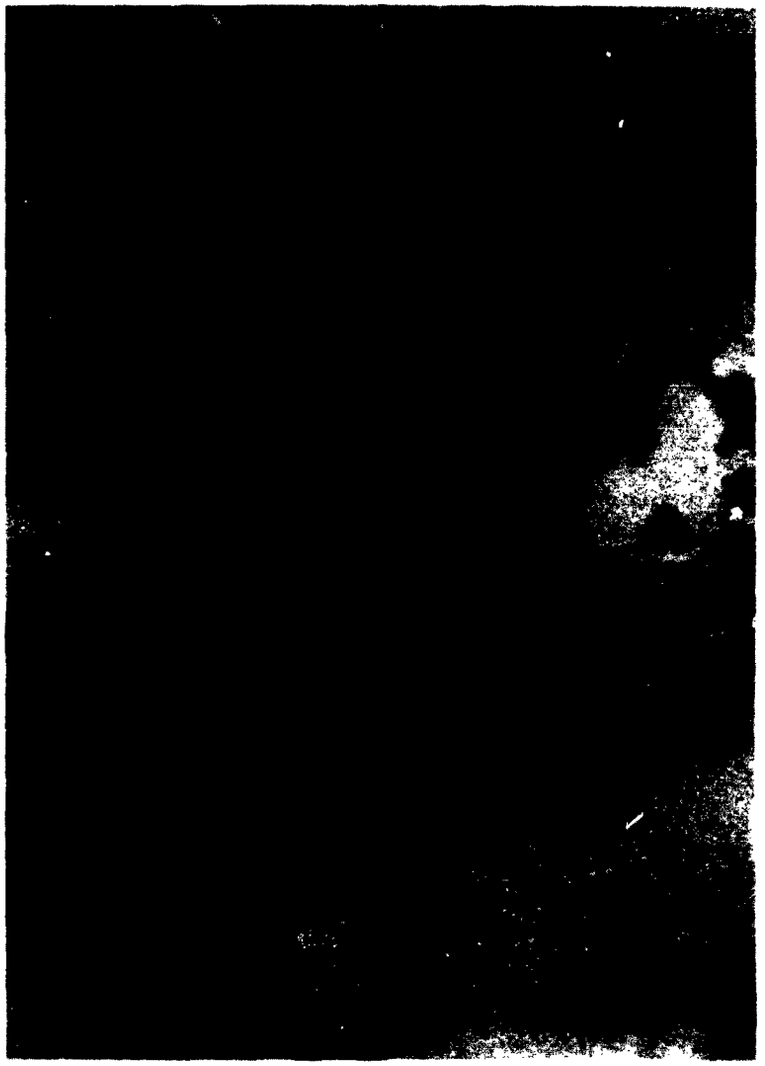

Figure 14. Photomacrograph of Spherical Reaction Products Collected from an Experiment with Oxygen (Run 27)

Magnification 70X

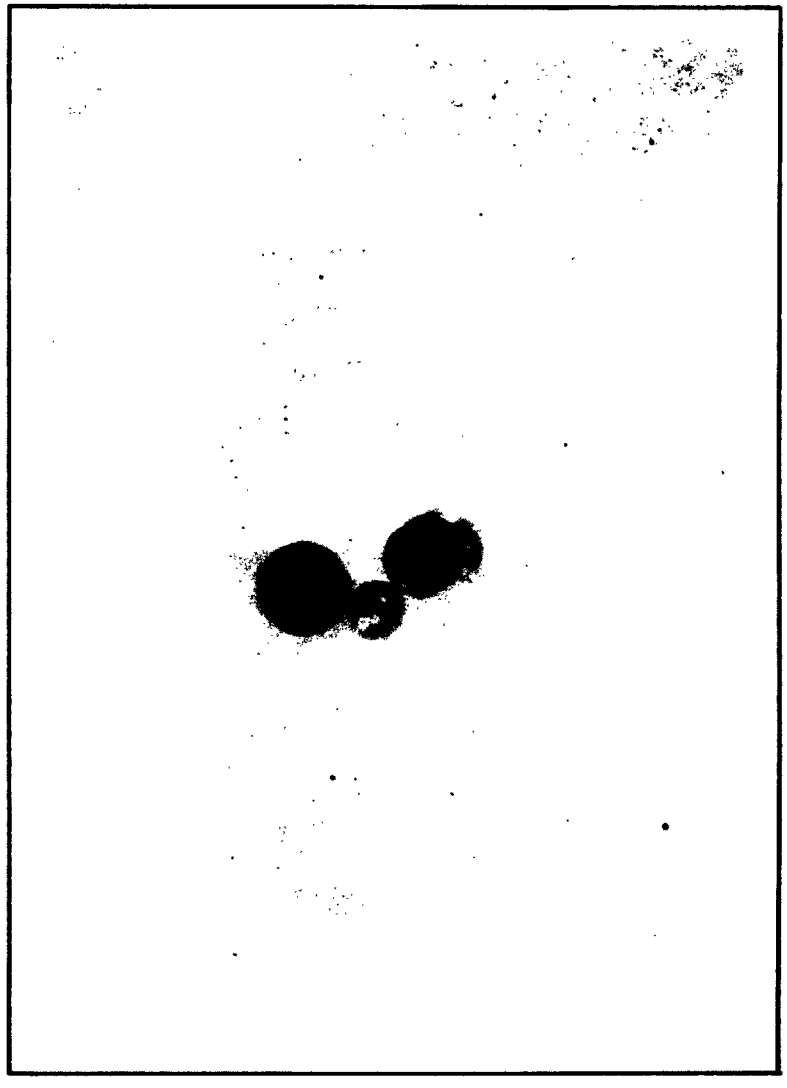

Figure 15. Photomacrograph of Three Types of Oxidized Reaction Products Collected from Run 27

Magnification 80X

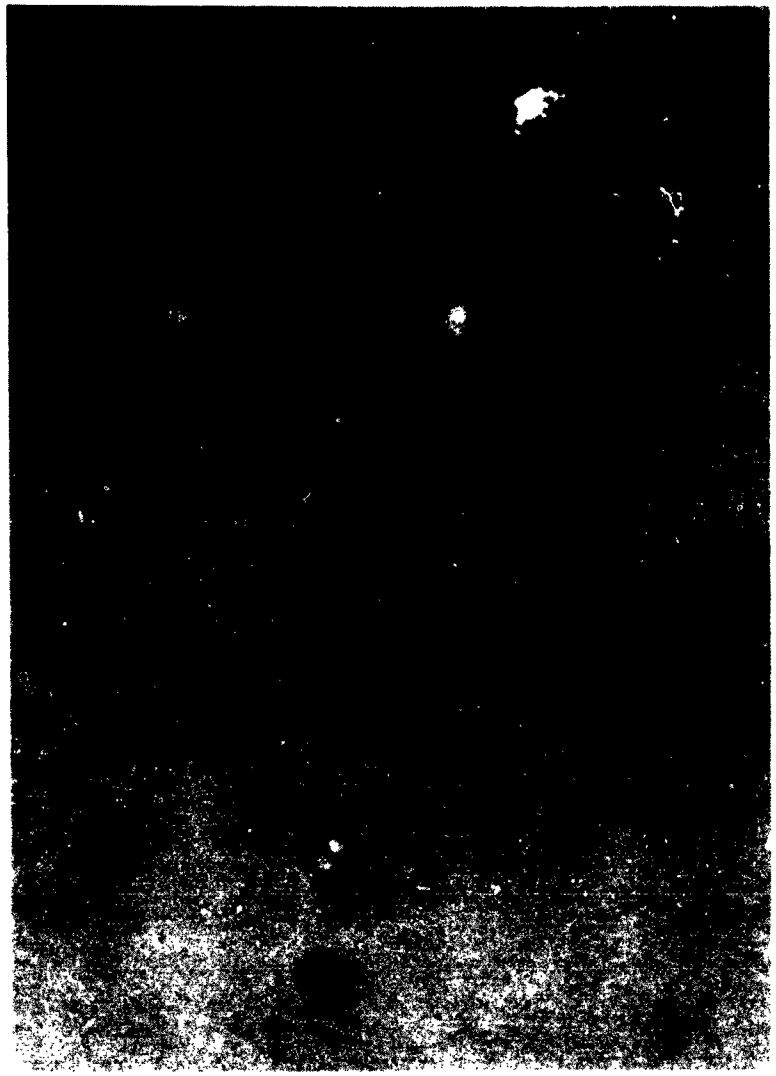

Figure 16. Photomacrograph Illustrating the Hollow Expanded Products Collected During Run 68

Magnification 70X

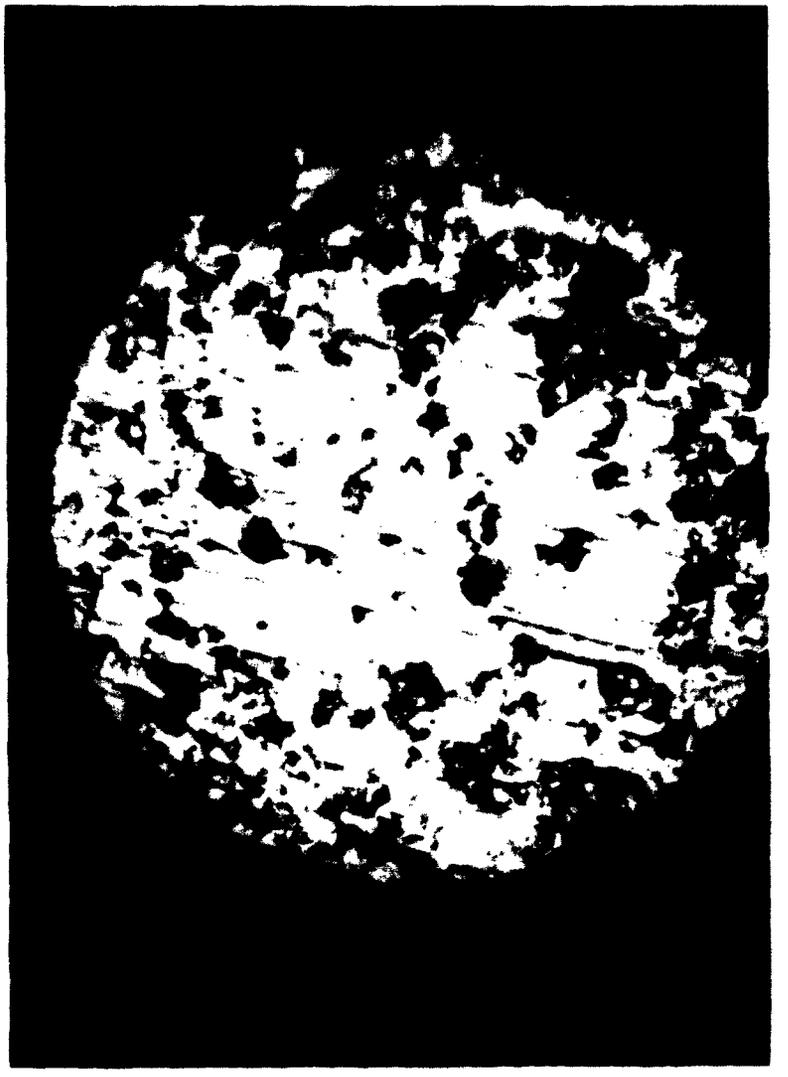

Figure 17. Photomicrograph Illustrating Complete Oxidation (Run 29). Note the oxide sphere with typical porosity.

Magnification 700X

Figure 18. Photomicrograph Illustrating Complete Oxidation and Hollow Center (Run 29)

Magnification 700X

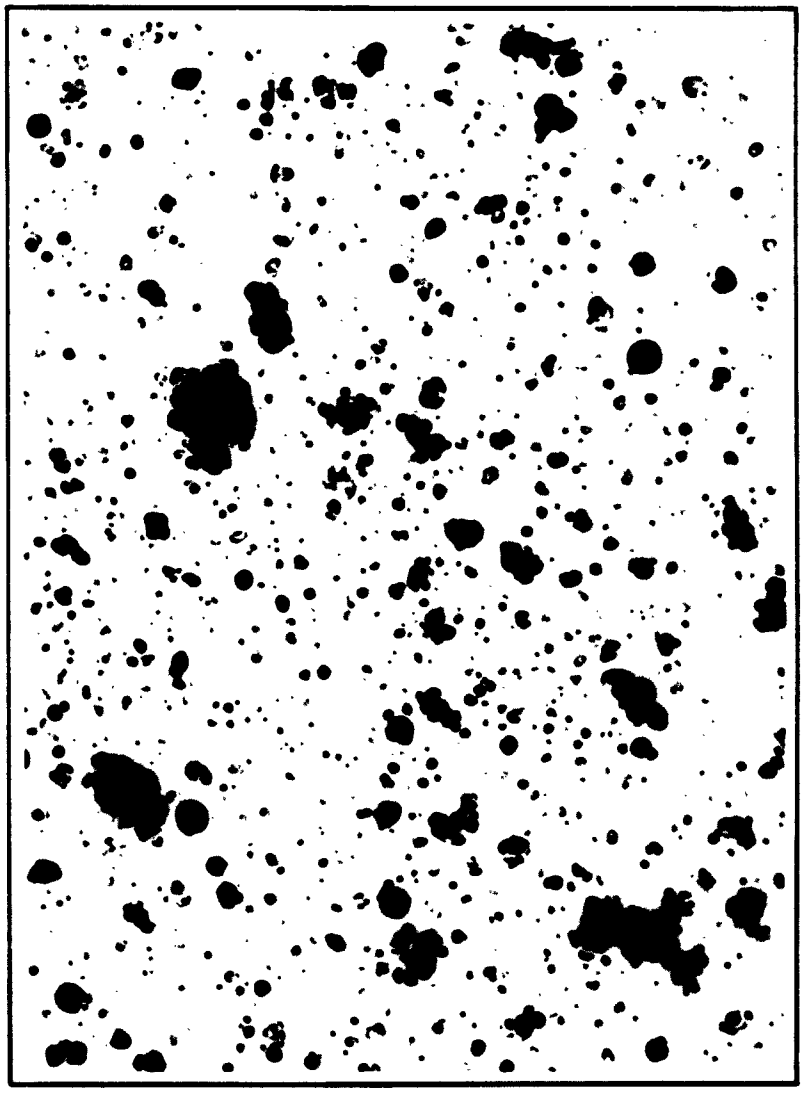

Figure 19. Electron Micrograph of Zr Hydride-10% U Particles Collected on a Grid with Collodion Coating (Run 24)

Direct Magnification 15,000X
Enlarged Magnification 45,000X

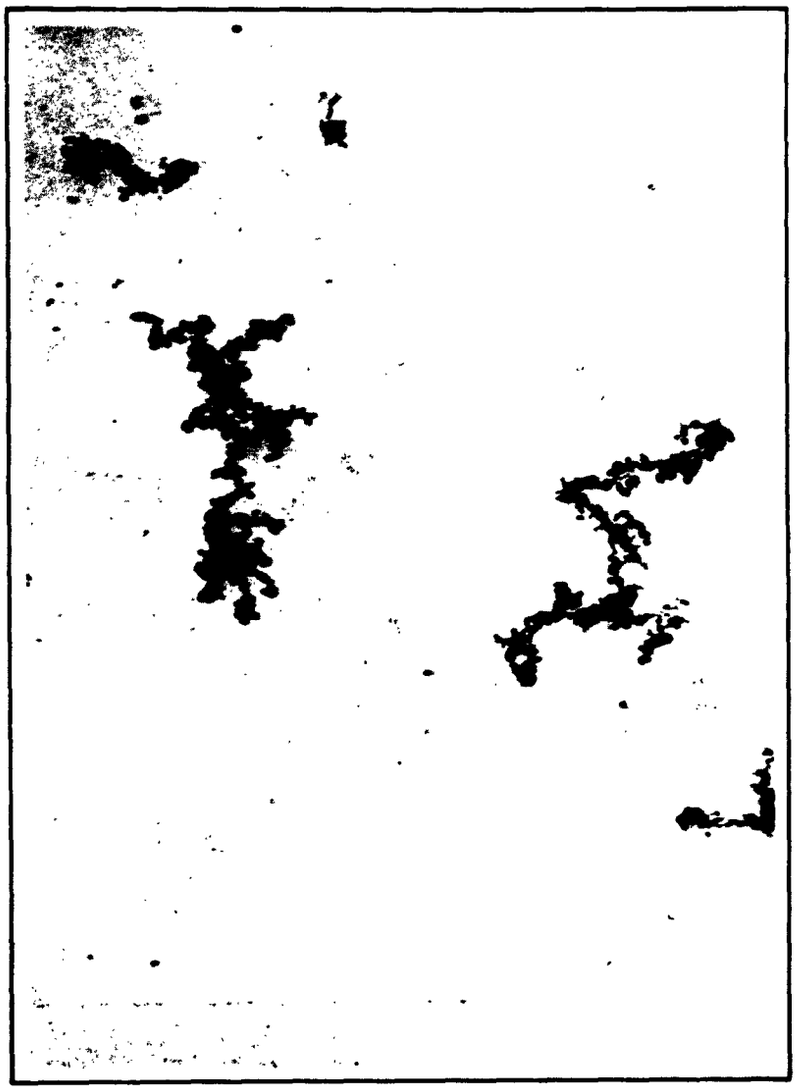

Figure 20. Electron Micrograph of Fine Dust Mounted on a Grid with Collodion Coating (72)

Direct Magnification 15,000X
Enlarged Magnification 45,000X

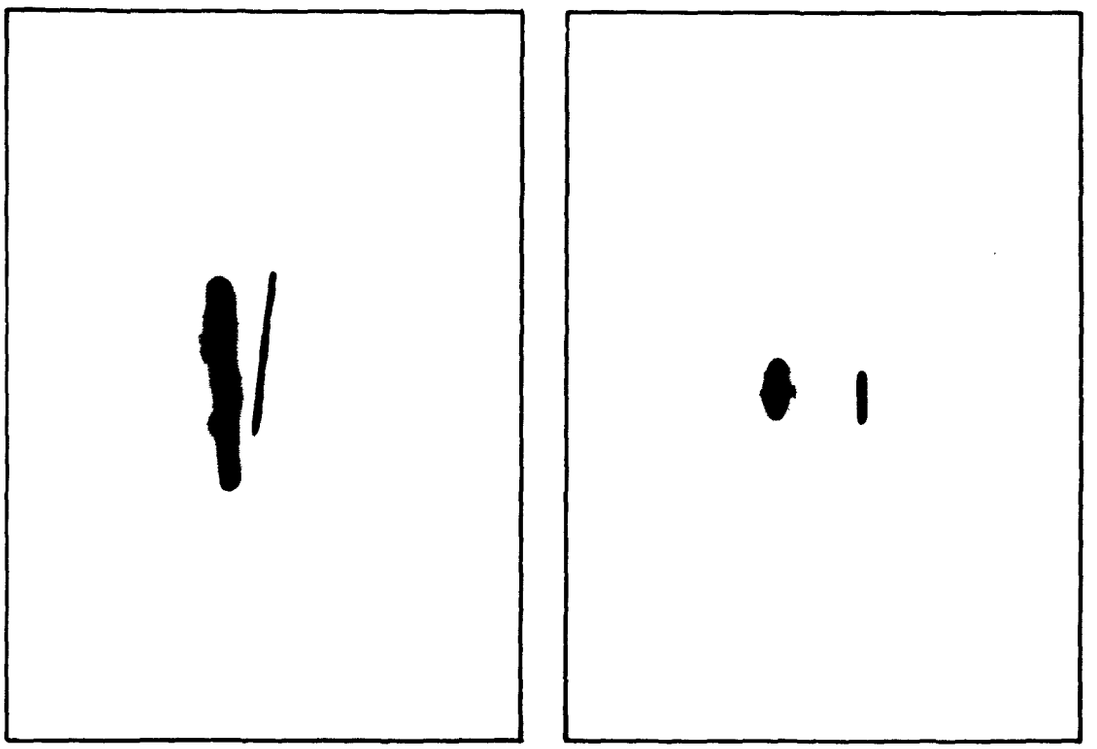

Figure 21. Typical Photographs of Particles Undergoing Ablation and Vapor-Phase Combustion (Run 28). The tracks on the right are reflections from the glass wall.

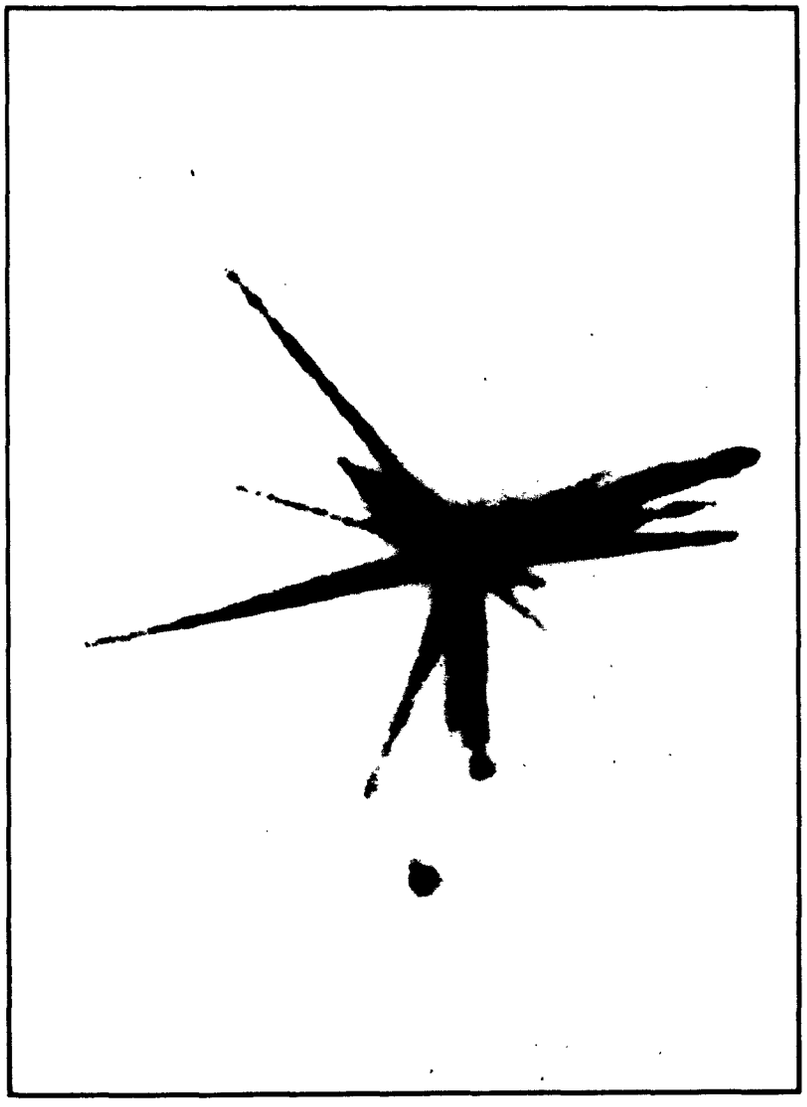

Figure 22. Photograph of a Typical Particle Explosion (Run 20)

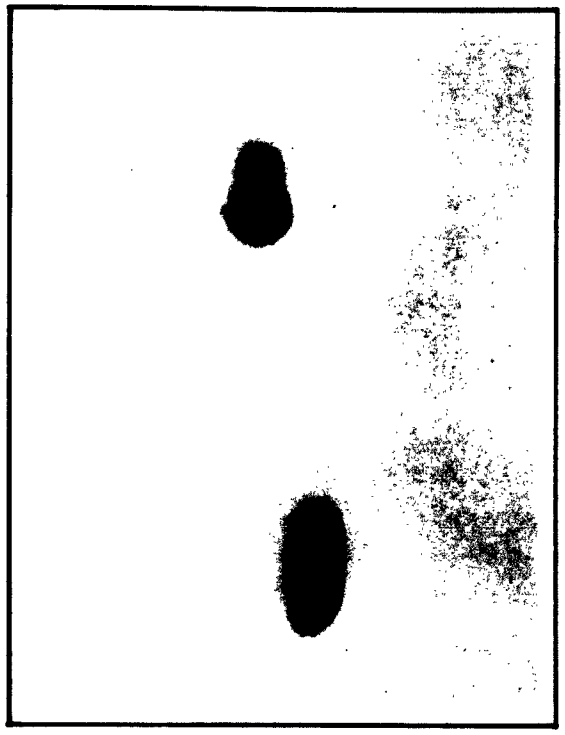

(a.)

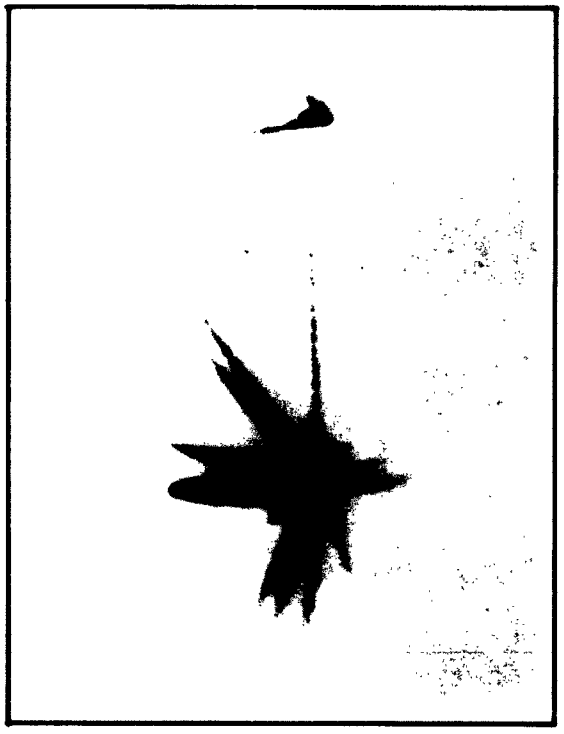

(b.)

Figure 23. Explosion Sequence of a Single Particle a. Upper Particle Swelling b. Same Particle Exploding (Run 20)

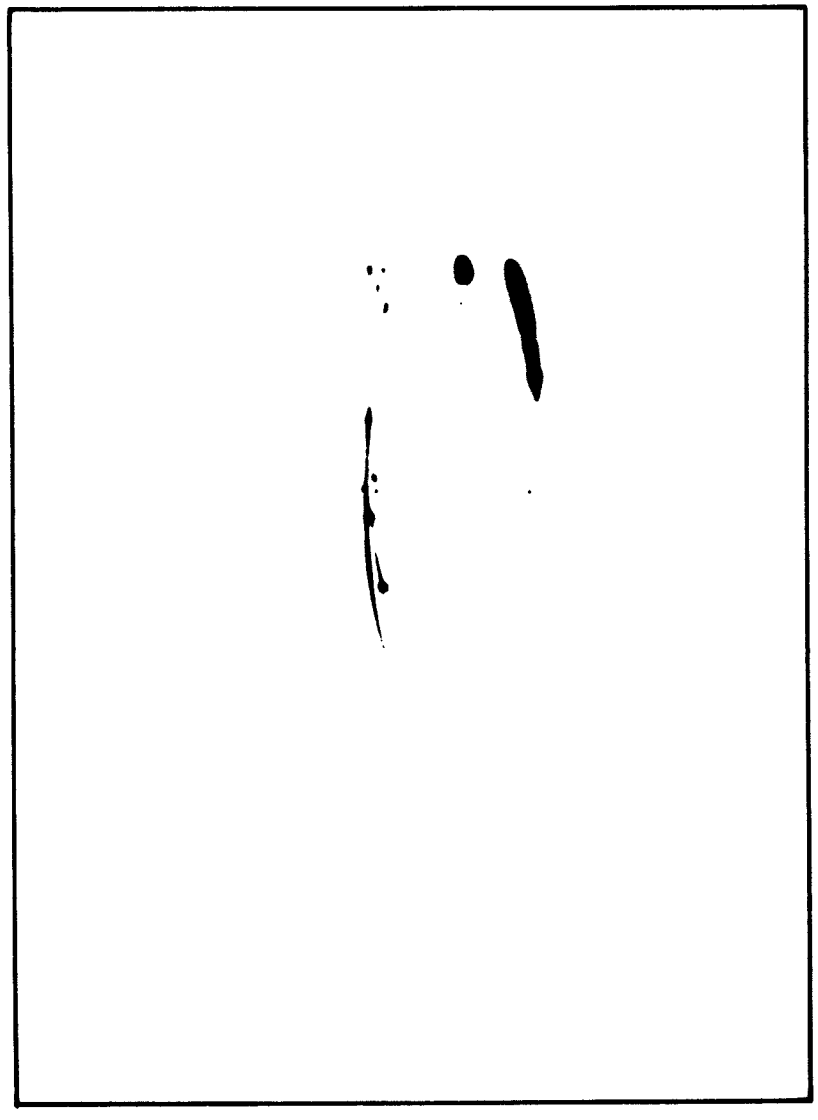

Figure 24. Photograph of a Particle Which Experienced Multiple Explosions (Track on Left) (Run 62)

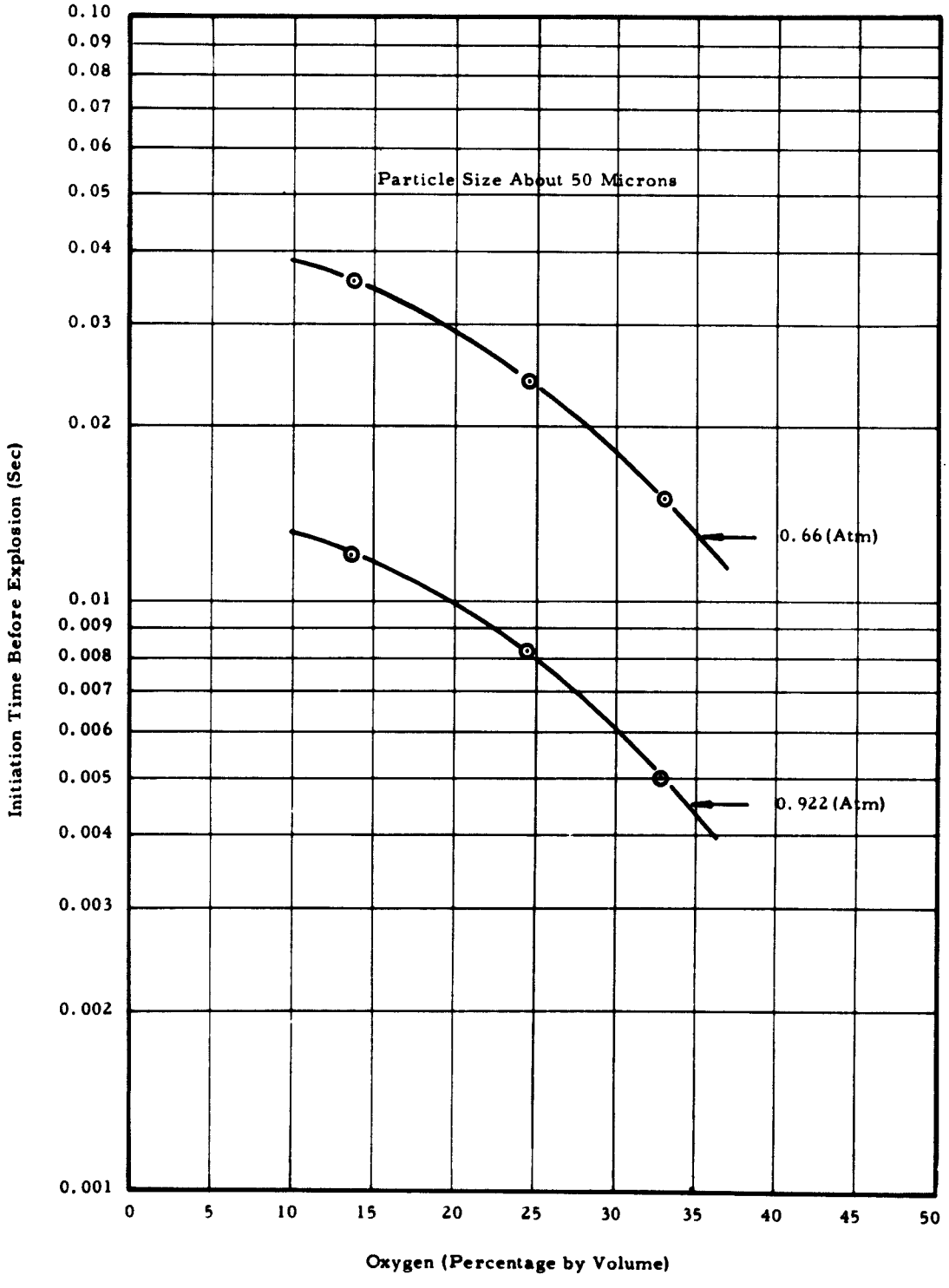

Figure 25. Initiation Time Before Explosion vs Oxygen Percentage at Constant Total Pressure

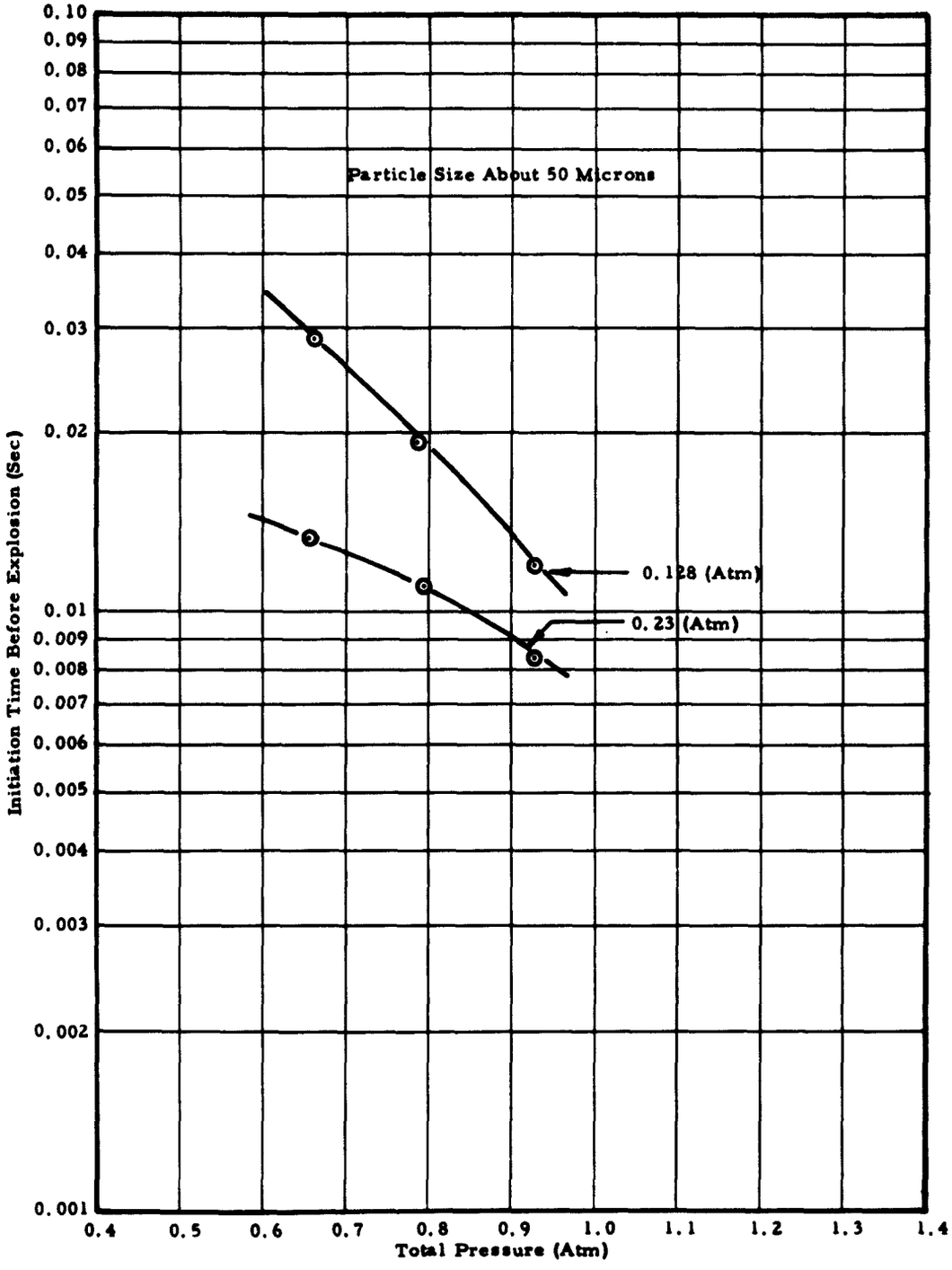

Figure 26. Initiation Time Before Explosion vs Total Pressure at Constant Oxygen Partial Pressure

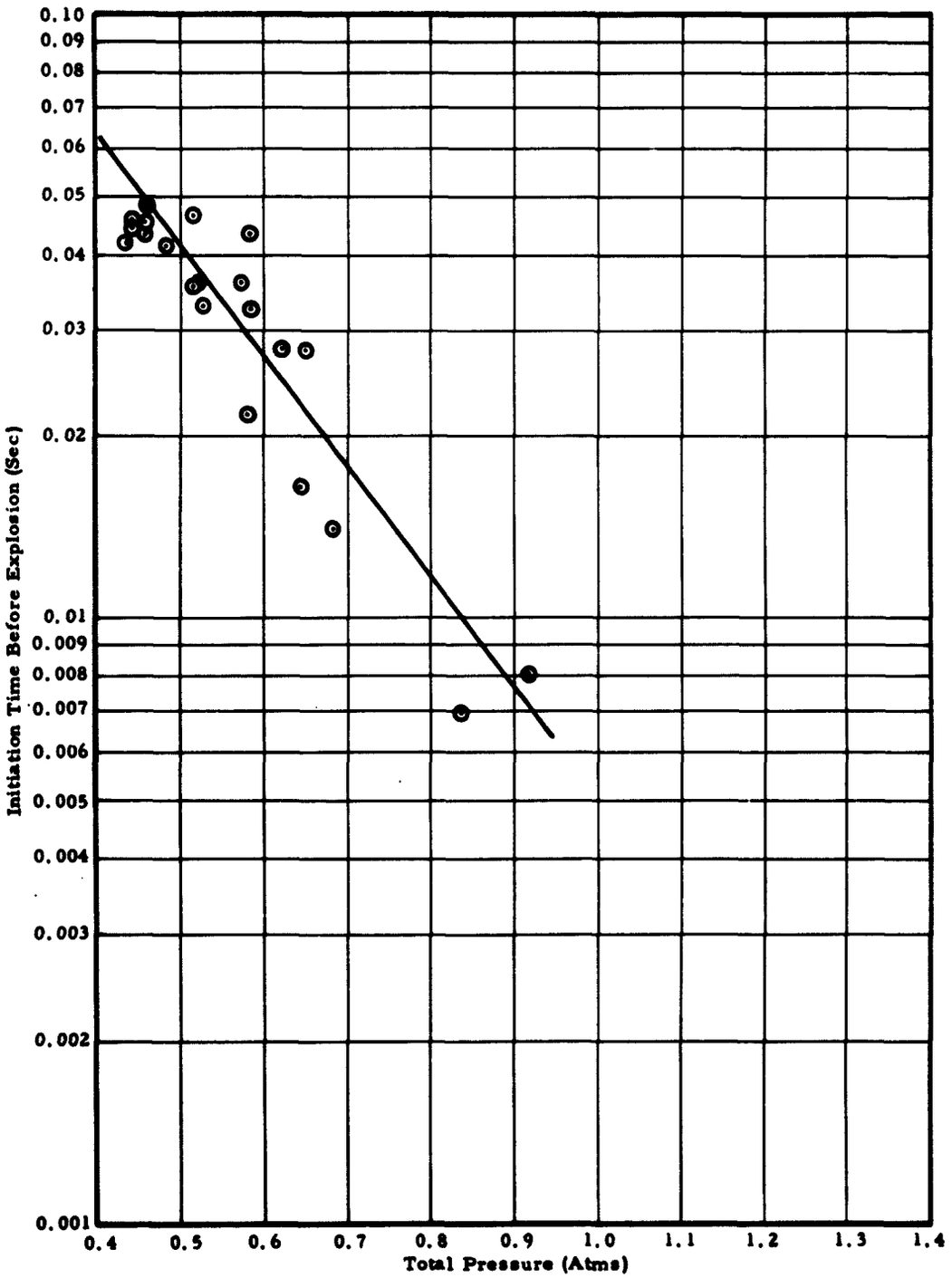

Figure 27. Initiation Time Before Explosion vs Total Pressure for a 79.059% Argon-20.9% Oxygen (by Volume) Atmosphere; Particle Size About 50 Microns

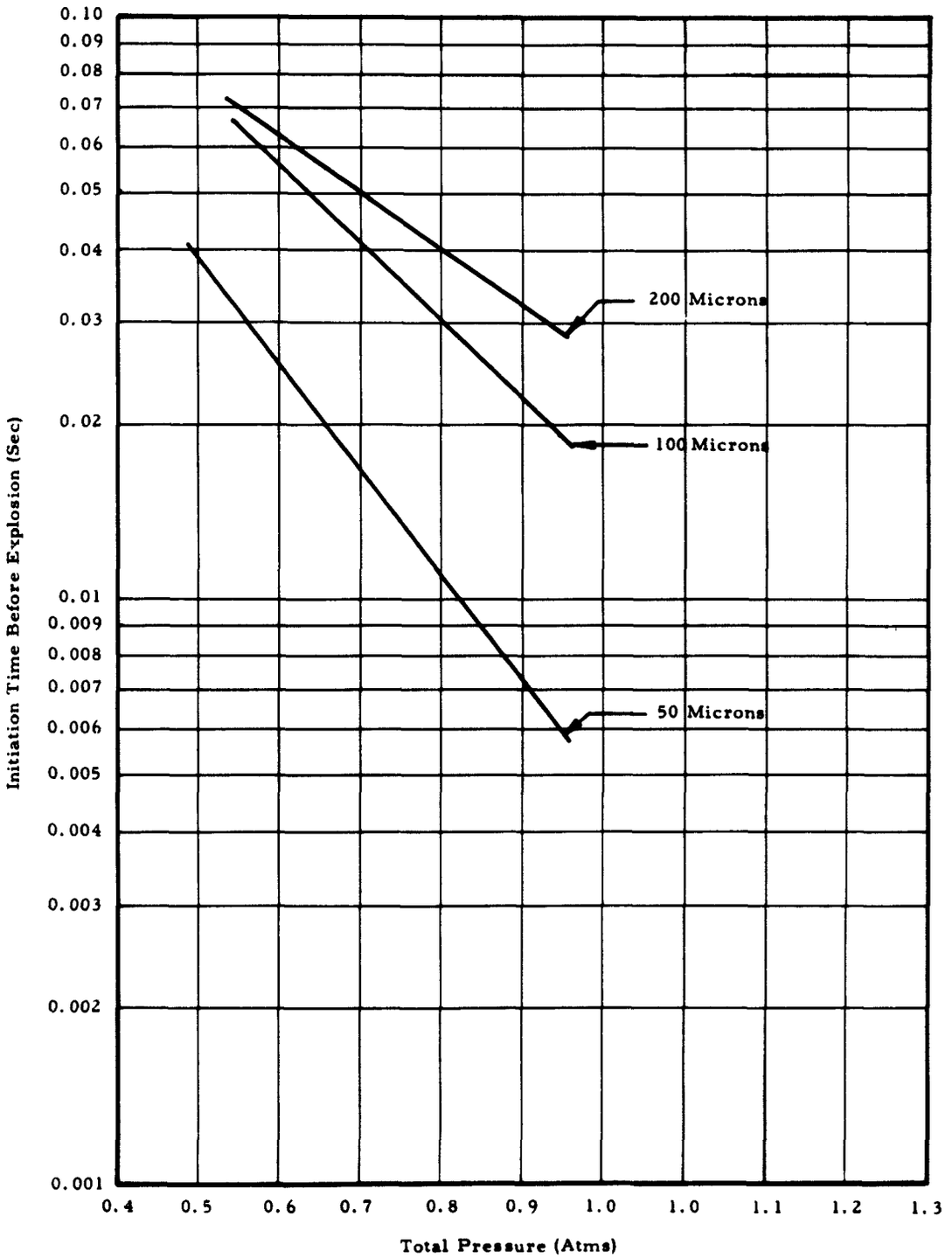

Figure 28. Initiation Time Before Explosion vs Total Pressure for a 79.059% Argon-20.95% Oxygen (by Volume) Atmosphere; Particle Sizes of About 50, 100, and 200 Microns

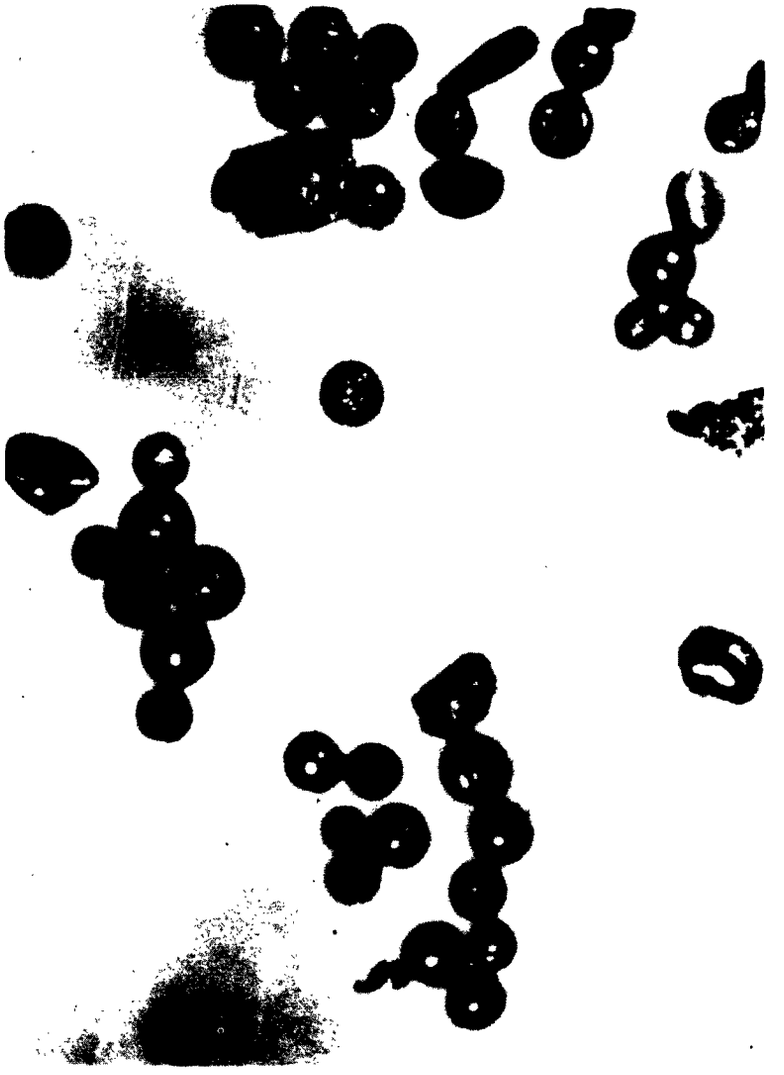

Figure 29. Photomacrograph of Spherical Products Collected from an Experiment During Which Nitrogen was Present (Run 65)

Magnification 60X

Figure 30. Photomicrograph Showing the Typical Microstructure of Nitrided Products from Figure 29. Note both smooth and irregular surfaces and grain boundary nitrides (Run 65)

Magnification 700X

APPENDIX

RESIDENCE TIME ANALYSIS

The experimental measurements of particle velocities were made at stations downstream from where the particles first entered the plenum (reaction) chamber. The following analysis was conducted in order to determine if the particles deccelerate significantly prior to the point of velocity measurement.

This analysis presents a general solution of the generalized Stokes equation. The results are applied to the case of a 50-micron sphere in an argon atmosphere at a temperature of 480°F. The calculations were made in the cgs unit system and converted to British units for final presentation.

The following symbols will be used throughout the calculation:

R = Reynolds number

K_d = Empirically derived drag coefficient

r = Particle radius

ρ_g = Argon density

ρ_P = Particle density

V = Particle velocity

μ = Coefficient of viscosity

m = Particle mass

F = Force on particle

From Dryden, Murnaghan, and Bateman*:

$$F = K_D \pi \rho_g V^2 r^2 \text{ (for spheres)} \qquad (1)$$

where

$$K_D = 14R^{-0.85} + 0.24$$

and

$$R = \frac{2 r V \rho_g}{\mu}$$

*H. L. Dryden, F. R. Murnaghan, and H. Bateman, Hydrodynamics, Dover Publications, Inc. (1956).

The drag equation is said to be valid for $0.2 < R < 200,000$. In the case under consideration:

$$R_{min} = \frac{2r_{min} V_{min} \rho_{g_{min}}}{\mu} \cong 14 > 0.2$$

The equation is therefore expected to hold for the case under consideration. Substituting $F = m\dot{V}$ into Equation 1:

$$M\dot{V} = -K_D \pi \rho_g V^2 r^2 = -(14R^{-0.85} + 0.24) \pi \rho_g V^2 r^2 \qquad (2)$$

where

$$M = \frac{4}{3} \pi \rho_P R^3$$

Substituting and rearranging:

$$\dot{V} = -\left(\frac{14}{\left[\frac{2r\rho_g}{\mu}\right]^{0.85} V^{0.85}} + 0.24\right)\left(\frac{3}{4}\right)\left(\frac{\rho_g}{\rho_P}\right)\left(\frac{V^2}{r}\right) \qquad (3)$$

or

$$\dot{V} = -K_1 \left[K_2 V^{1.15} + 0.24 V^2\right] \qquad (4)$$

where

$$K_1 \equiv \frac{3}{4} \frac{\rho_g}{\rho_P r}$$

and

$$K_2 \equiv 14 \left(\frac{\mu}{2r\rho_g}\right)^{0.85}$$

Integrating:

$$K_1 t = -\int \frac{dV}{K_2 V^{1.15} + 0.24 V^2} = -\int \frac{dV}{V(K_2 V^{0.15} + 0.24 V)}$$

This integral is difficult to evaluate without numerical values. However, approximating $1/(K_2 V^{0.15} + 0.24V)$ by $1/(aV + b)$ will yield an evaluation using elementary functions. The approximation is accomplished by fitting a straight line through the graph of $(K_2 V^{0.15} + 0.24V)$ and then

obtaining the "a" and "b" of (av + b). Figure A-1a shows the fit of the curve for the case under consideration.

Having evaluated "a" and "b", the integral

$$\int_{V_o}^{V(t)} \frac{dv}{V(K_2 V^{0.15} + 0.24V)} \approx \int_{V_o}^{V(t)} \frac{dv}{V(aV + b)} \tag{5}$$

may be evaluated, giving

$$K_i t = \frac{1}{b} \ln \left[\frac{(aV + b) V_o}{(aV_o + b) V} \right]$$

or

$$e^{K_1 bt} = \frac{(aV + b) V_o}{(aV_o + b) V} \tag{6}$$

Solving for V(t):

$$V(t) = \frac{bV_o}{e^{K_1 bt} (aV_o + b) - aV_o} \tag{7}$$

$$D(t) = \text{distance in time, } t = \int_o^t V(t)\, dt$$

$$D(t) = \frac{1}{aK_1} \ln \left| \frac{e^{K_1 bt} (aV_o + b) - aV_o}{b} \right| - \frac{bt}{a} \tag{8}$$

Thus, given the distance traveled, Equation 8 can be used to evaluate Vo at any t. Utilizing the values of Vo and t in Equation 7 will yield V at D. These two results are plotted against one another in Figure A-1b for the case under consideration. A curve is also included for the same conditions but assuming the drag forces to be negligible. For the 50-micron particles, the velocity is seen to vary from the constant velocity approximation by about 20%. In the case of 100- and 200-micron particles, the error associated with the constant velocity approximation is of the order of 6% and 2%, respectively.

The calculations were made for a gas pressure of 1 atm. The results of residence time can be corrected to any pressure P by the following equation:

$$t_P = t_{(\text{at one atm.})} (0.8 + 0.2P)$$

Thus, for $0.5 < P < 1.1$ atm, the maximum error is 10% for the 50-micron particles and in the order of 3% and 0.8% for the 100- and 200-micron particles, respectively.

The difference in viscosity between argon and argon-oxygen mixtures introduces a maximum error in the order of 1% and is thus negligible. Other errors such as gas velocity and argon temperature were also found to be negligible.

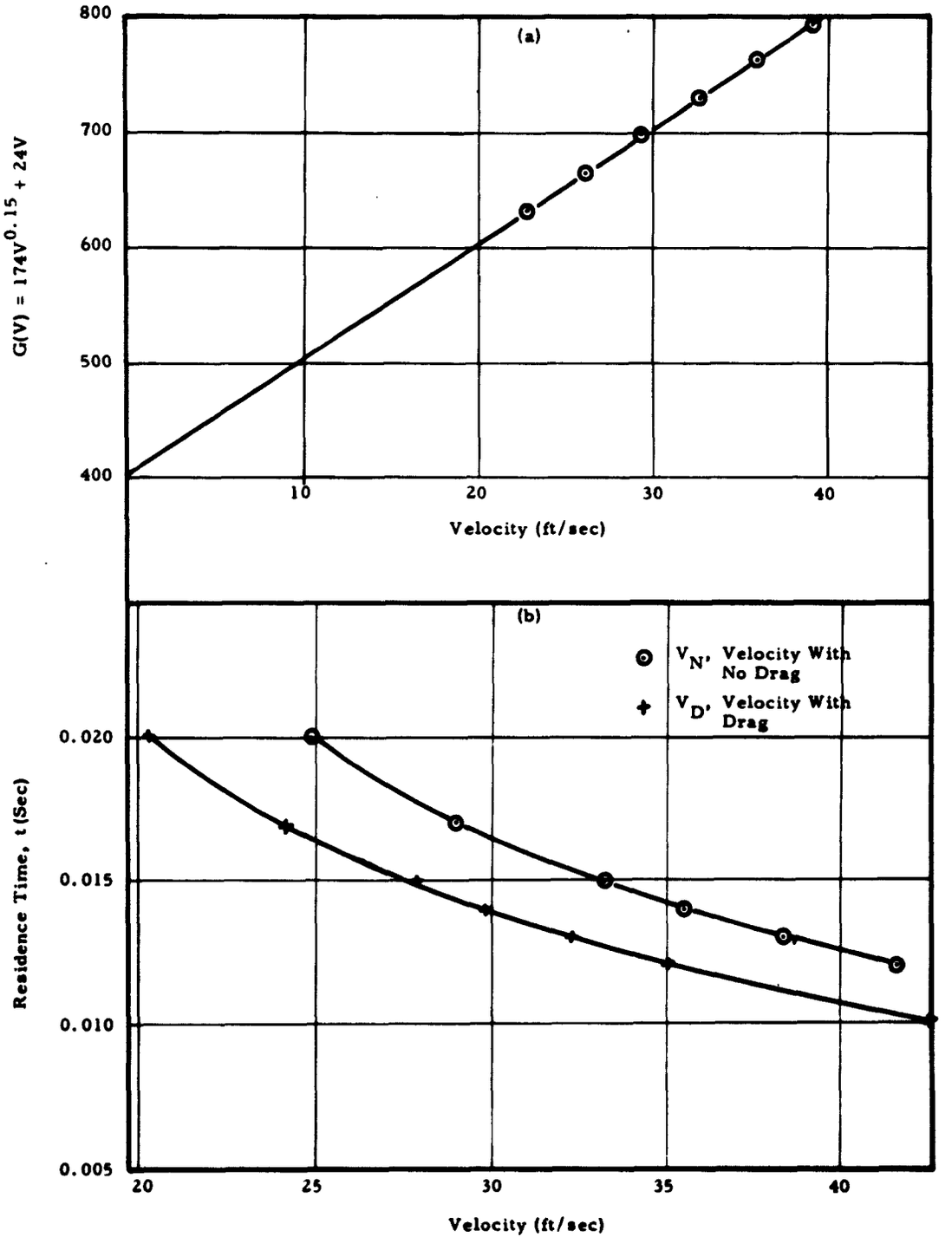

Figure A-1. Equation Approximation Curves

DISTRIBUTION

No. Cys

HEADQUARTERS USAF

1 USAF Dep, The Inspector General (AFIDI), Norton AFB, Calif
1 USAF Directorate of Nuclear Safety (AFINS), Kirtland AFB, NM

MAJOR AIR COMMANDS

1 AUL, Maxwell AFB, Ala

AFSC ORGANIZATIONS

SSD, AF Unit Post Office, Los Angeles 45, Calif
2 (SSTRE)
1 (SSZMS)

KIRTLAND AFB ORGANIZATIONS

1 AFSWC (SWEH), Kirtland AFB, NM
AFWL, Kirtland AFB, NM
60 (WLL)
1 (WLRP)
2 (WLDN-1)
2 (WLDN-2)

OTHER AIR FORCE AGENCIES

6 Director, USAF Project RAND, via: Air Force Liaison Office, The RAND Corporation, ATTN: Miss Mary Romig, 1700 Main Street, Santa Monica, Calif

NAVY ACTIVITIES

1 US Naval Weapons Evaluation Facility (NWEF) (Code 404), Kirtland AFB, NM

DISTRIBUTION (Cont'd)

No. Cys	
	OTHER DOD ACTIVITIES
	Director, Advanced Research Projects Agency, Department of Defense, The Pentagon, Wash 25, DC
2	(Lt. Col. Ray Weidler)
2	(Mr. James E. Blower)
20	Hq Defense Documentation Center for Scientific and Technical Information (DDC), Arlington Hall Sta, Arlington 12, Va
	AEC ACTIVITIES
	US Atomic Energy Commission, Wash 25, DC
4	(Asst Director for Compact Reactor Systems DRD)
4	(Asst Director for Nuclear Safety DRD)
1	US Atomic Energy Commission, Canoga Park Area Office, ATTN: Manager, Canoga Park Area Office, Mr. J. Levy, P.O. Box 591, Canoga Park, Calif
3	Sandia Corporation, ATTN: Mr. V. E. Blake, Department 7110, Sandia Base, NM
1	University of California Lawrence Radiation Laboratory, ATTN: Mr. Clovis Craig, P. O. Box 808, Livermore, Calif
	OTHER
1	OTS, Department of Commerce, Wash 25, DC
3	Battelle Memorial Institute, ATTN: E. L. Foster, 505 King Avenue, Columbus, Ohio
1	Institute of the Aerospace Sciences, Inc., 2 East 64th Street, New York 21, NY
10	General Dynamics/Astronautics, ATTN: Mr. E. J. P. Philbin, P. O. Box 1128, Mail Zone 596-2, San Diego 12, Calif
3	Stanford Research Institute, ATTN: Dr. Fred Littman, Menlo Park, Calif
3	Vidya Research and Development, ATTN: Mr. W. J. Fleming, 2626 Hanover Street, Palo Alto, Calif
12	Astropower, ATTN: Dr. A. E. Levy-Pascal, 2968 Randolph Avenue, Costa Mesa, Calif
3	Westinghouse Electric Corp., Astronuclear Laboratory, ATTN: Mr. Alexander L. Feild, Jr. 250 Mt Lebanon Blvd, Pittsburgh, Pa

DISTRIBUTION (Cont'd)

No. Cys	
3	Armour Research Foundation, ATTN: Mr. Alexander Goldsmith, 10 West 35th Street, Chicago 16, Ill
3	Space Information Systems Division, North American Aviation Inc., 12214 Lakewood Blvd., Downey, Calif, ATTN: Mr. Mark Morris, Dept 468
3	AVCO Corp., 201 Lowell St, Wilmington, Mass
3	General Technologies Corp., ATTN: Mr. J. D. Graves, 2302 Willowood Lane, Alexandria, Va
2	Aerojet-General Nucleonics, ATTN: Mr. J. P. Lehman, Fostoria Way, San Ramon, Calif
6	Aerospace Corp., (Tech Library Documents Group, ATD 61-5720 Technical Information Center), P. O. Box 95085, Los Angeles, Calif
1	Official Record Copy (WLDN-2, Mr. Ungvarsky)

Air Force Special Weapons Center, Kirtland AF Base, New Mexico
Rpt No. AFSWC-TDR-63-51. PARTICLE DISINTEGRATION STUDY FOR RE-ENTERING NUCLEAR AUXILIARY POWER SYSTEMS. Final report, June 1963. 76 p. incl illus, tables, 20 refs.

Unclassified Report

The purpose of this study was to determine the chemical history and related physical phenomena of liquid Zr-U droplets in the presence of a flowing mixture of atmospheric gases at various partial pressures.

A theoretical analysis of the aerodynamic and thermodynamic conditions affecting the droplets was carried out. Experimental investigation was conducted on the interaction of particles of 50- to 200-micron size with oxygen and nitrogen at different concentrations and total pressures.

1. NAP
2. Oxidation
3. Particle physics
4. Particle trajectories
5. Reactor fuels -- decay
6. Uranium alloys -- decay
7. Zirconium alloys -- decay

I. AFSC Project 1831, Task 183101
II. Contract AF 29(601)-5004
III. Astropower, Inc., Newport Beach, Calif.
IV. A.E. Levy-Pascal, L.E. Bell, R.R. Koppang, A.H. Malinovsky, S.W. Pohl, R. Silvestri, and N.A. Tiner
V. In DDC collection

Air Force Special Weapons Center, Kirtland AF Base, New Mexico
Rpt No. AFSWC-TDR-63-51. PARTICLE DISINTEGRATION STUDY FOR RE-ENTERING NUCLEAR AUXILIARY POWER SYSTEMS. Final report, June 1963. 76 p. incl illus, tables, 20 refs.

Unclassified Report

The purpose of this study was to determine the chemical history and related physical phenomena of liquid Zr-U droplets in the presence of a flowing mixture of atmospheric gases at various partial pressures.

A theoretical analysis of the aerodynamic and thermodynamic conditions affecting the droplets was carried out. Experimental investigation was conducted on the interaction of particles of 50- to 200-micron size with oxygen and nitrogen at different concentrations and total pressures.

1. NAP
2. Oxidation
3. Particle physics
4. Particle trajectories
5. Reactor fuels -- decay
6. Uranium alloys -- decay
7. Zirconium alloys -- decay

I. AFSC Project 1831, Task 183101
II. Contract AF 29(601)-5004
III. Astropower, Inc., Newport Beach, Calif.
IV. A.E. Levy-Pascal, L.E. Bell, R.R. Koppang, A.H. Malinovsky, S.W. Pohl, R. Silvestri, and N.A. Tiner
V. In DDC collection

Air Force Special Weapons Center, Kirtland AF Base, New Mexico
Rpt No. AFSWC-TDR-63-51. PARTICLE DISINTEGRATION STUDY FOR RE-ENTERING NUCLEAR AUXILIARY POWER SYSTEMS. Final report, June 1963. 76 p. incl illus, tables, 20 refs.

Unclassified Report

The purpose of this study was to determine the chemical history and related physical phenomena of liquid Zr-U droplets in the presence of a flowing mixture of atmospheric gases at various partial pressures.

A theoretical analysis of the aerodynamic and thermodynamic conditions affecting the droplets was carried out. Experimental investigation was conducted on the interaction of particles of 50- to 200-micron size with oxygen and nitrogen at different concentrations and total pressures.

1. NAP
2. Oxidation
3. Particle physics
4. Particle trajectories
5. Reactor fuels -- decay
6. Uranium alloys -- decay
7. Zirconium alloys -- decay

I. AFSC Project 1831, Task 183101
II. Contract AF 29(601)-5004
III. Astropower, Inc., Newport Beach, Calif.
IV. A.E. Levy-Pascal, L.E. Bell, R.R. Koppang, A.H. Malinovsky, S.W. Pohl, R. Silvestri, and N.A. Tiner
V. In DDC collection

Air Force Special Weapons Center, Kirtland AF Base, New Mexico
Rpt No. AFSWC-TDR-63-51. PARTICLE DISINTEGRATION STUDY FOR RE-ENTERING NUCLEAR AUXILIARY POWER SYSTEMS. Final report, June 1963. 76 p. incl illus, tables, 20 refs.

Unclassified Report

The purpose of this study was to determine the chemical history and related physical phenomena of liquid Zr-U droplets in the presence of a flowing mixture of atmospheric gases at various partial pressures.

A theoretical analysis of the aerodynamic and thermodynamic conditions affecting the droplets was carried out. Experimental investigation was conducted on the interaction of particles of 50- to 200-micron size with oxygen and nitrogen at different concentrations and total pressures.

1. NAP
2. Oxidation
3. Particle physics
4. Particle trajectories
5. Reactor fuels --decay
6. Uranium alloys -- decay
7. Zirconium alloys -- decay

I. AFSC Project 1831, Task 183101
II. Contract AF 29(601)-5004
III. Astropower, Inc., Newport Beach, Calif.
IV. A.E. Levy-Pascal, L.E. Bell, R.R. Koppang, A.H. Malinovsky, S.W. Pohl, R. Silvestri, and N.A. Tiner
V. In DDC collection

The results obtained indicate that the droplets undergo partial or complete oxidation or nitridation, depending on experimental conditions. Only when oxygen was present did the droplets disintegrate into submicron particles. The frequency and mode of disintegration depend on the total pressure, oxygen concentration, and particle size; however, specific variables should be further investigated in order to reach more quantitative and realistic conclusions.		The results obtained indicate that the droplets undergo partial or complete oxidation or nitridation, depending on experimental conditions. Only when oxygen was present did the droplets disintegrate into submicron particles. The frequency and mode of disintegration depend on the total pressure, oxygen concentration, and particle size; however, specific variables should be further investigated in order to reach more quantitative and realistic conclusions.	
The results obtained indicate that the droplets undergo partial or complete oxidation or nitridation, depending on experimental conditions. Only when oxygen was present did the droplets disintegrate into submicron particles. The frequency and mode of disintegration depend on the total pressure, oxygen concentration, and particle size; however, specific variables should be further investigated in order to reach more quantitative and realistic conclusions.		The results obtained indicate that the droplets undergo partial or complete oxidation or nitridation, depending on experimental conditions. Only when oxygen was present did the droplets disintegrate into submicron particles. The frequency and mode of disintegration depend on the total pressure, oxygen concentration, and particle size; however, specific variables should be further investigated in order to reach more quantitative and realistic conclusions.	